

January 2008

# Phase Transitions in Charged Topological-AdS Black Holes

George Koutsoumbas\*, Eleftherios Papantonopoulos<sup>b</sup>

*Department of Physics, National Technical University of Athens,  
Zografou Campus GR 157 73, Athens, Greece*

and

George Siopsis<sup>‡</sup>

*Department of Physics and Astronomy, The University of Tennessee,  
Knoxville, TN 37996 - 1200, USA*

## Abstract

We study the perturbative behaviour of charged topological-AdS black holes. We calculate both analytically and numerically the quasi-normal modes of the electromagnetic and gravitational perturbations. Keeping the charge-to-mass ratio constant, we show that there is a second-order phase transition at a critical temperature at which the mass of the black hole vanishes. We pay special attention to the purely dissipative modes appearing in the spectrum as they behave singularly at the critical point.

\* kutsbas@central.ntua.gr

<sup>b</sup> lpapa@central.ntua.gr

<sup>‡</sup> siopsis@tennessee.edu

## 1 Introduction

It is well known that if a black hole is initially perturbed, the surrounding geometry will start vibrating into quasi-normal oscillation modes, whose frequencies and decay times depend only on the intrinsic features of the black hole itself, being insensitive to the details of the initial perturbation. The radiation associated with these modes is expected to be seen with gravitational wave detectors in the coming years, giving valuable information on the properties of black holes. For these reasons, quasi-normal modes (QNMs) of black holes in asymptotically flat spacetimes have been extensively studied (for reviews, see [1, 2]).

The Anti-de Sitter - conformal field theory (AdS/CFT) correspondence has led to an intensive investigation of black hole QNMs in asymptotically AdS spacetimes. Quasi-normal modes in AdS spacetime were first computed for a conformally invariant scalar field, whose asymptotic behaviour is similar to flat spacetime [3]. Subsequently, motivated by the AdS/CFT correspondence, Horowitz and Hubeny made a systematic computation of QNMs for scalar perturbations of Schwarzschild-AdS (S-AdS) spacetimes [4]. Their work was extended to electromagnetic and gravitational perturbations of S-AdS black holes in [5]. The study of scalar perturbations was further extended to the case of Reissner-Nordström-AdS (RN-AdS) black holes in [6]. Finally, the QNMs of scalar, electromagnetic and gravitational perturbations of RN-AdS black holes were presented in [7] using the results of [8].

The QNMs of AdS black holes have an interpretation in terms of the dual conformal field theory (CFT) [10]. According to the AdS/CFT correspondence, a large static black hole in AdS corresponds to an (approximately) thermal state in the CFT. Perturbing the black hole corresponds to perturbing this thermal state, and the decay of the perturbation describes the return to thermal equilibrium. So we obtain a prediction for the thermalization timescale in the strongly coupled CFT. In ref. [4] it was shown that the QNMs for the scalar perturbations of large Schwarzschild-AdS black holes scaled with the temperature and it was argued that the perturbed system in the dual description will approach to thermal equilibrium of the boundary conformal field theory. However, when the black hole size is comparable to the AdS length scale there is a clear departure from this behaviour. It was then conjectured that this behaviour may be connected with a Hawking-Page phase transition [11, 12] which occurs when the temperature lowers.

These results were further confirmed in [5, 6, 7, 9]. However, the behaviour of QNMs for small black holes is still poorly understood. Another interesting finding of the electromagnetic and gravitational perturbations is that purely dissipative modes appear in the spectrum which are pure imaginary QNMs. In such perturbed classical backgrounds the presence of these dissipative modes indicate that the boundary theory reaches thermal equilibrium with no oscillations. It was shown in [5] that for axial perturbations of Schwarzschild-AdS black holes these highly damped modes scale as the inverse of the black hole radius and this behaviour persisted in the case of Reissner-Nordström-AdS black holes [7].

It was observed in [13] that for small black holes as we lower the temperature to a critical value there is a phase transition of a vacuum topological black hole towards a hairy black hole (MTZ). This claim was supported in [14] by calculating the QNMs of electromagnetic

perturbations of the MTZ black hole and topological black holes. It was found that there is a change in the slope of the QNMs as we decrease the value of the horizon radius below a critical value, and this change has been attributed to the phase transition. It was also observed in [14] that for small black holes the quasi-normal frequencies converge toward the imaginary axis, i.e., their real part decreases and after the first few quasi-normal frequencies, it vanishes, indicating that for black hole radius smaller than the AdS length scale there are only a finite number of QNMs. It was shown that the finite number of such modes for small horizons is due to the existence of bound states behind the horizon, which is an unobservable region. Further evidence that the behaviour of QNMs may provide indications of a phase transition was provided in [15].

Topological black holes [16]-[25], having hyperbolic horizons, introduce new features not present in spherical black holes. In [26] it was shown that hyperbolic black holes can be described as thermal Rindler states of the dual conformal field theory in flat space. It was also found that, for small topological black holes of the size of the AdS length scale, the entropy at strong coupling is larger than the entropy obtained from field theory at lowest perturbation order at weak coupling. One possible explanation put forward was that there is a phase transition of topological black hole to vacuum AdS space at a critical temperature, which however was not observed in [26] (see also [20, 27]).

In this work we make a detailed study of electromagnetic and gravitational perturbations of charged topological black holes (CTBH) in AdS space. Studying these perturbations of the background geometry, we show that the second-order phase transition observed at a critical temperature in [14] occurs in more general configurations including charge. We calculate both analytically and numerically the QNMs of axial and in some cases the polar perturbations of large and small black holes. We find that for large black holes the QNMs irrespectively of the value of the charge, exhibit a negative slope. However, if the value of the black hole radius is smaller than the AdS length scale and the charge is small, the propagating QNMs (whose frequencies have a non-vanishing real part) of both axial and polar perturbations are finite with a positive slope. We attribute this behaviour to a second order phase transition which occurs as the temperature approaches a critical value (or the black hole radius is approaching the length scale of the AdS space). We also find that, in the case of small black holes, if we increase the charge, the number of propagating QNMs is again infinite and a part of positive slope coexists with the negative slope frequencies. This observation indicates that in the case of small black holes, the charge plays the rôle of an order parameter and according to the AdS/CFT correspondence we expect that the dual boundary theory is described by a thermal state with coexisting phases.

We also study the purely dissipative modes appearing in the spectrum, both analytically and numerically of electromagnetic and gravitational perturbations of the charged topological black holes. For large black holes the purely dissipative modes of both axial and polar perturbations scale linearly with temperature. Also the intermediate black holes to a good approximation depend linearly on the temperature. This is the expected behaviour for large and intermediate black holes and they agree with the normal QNMs behaviour discussed in [4]. If the black hole radius is smaller than the AdS length scale then we find a clear departure from linearity with temperature. If the charge is small the purely dissipative modes scale with the temperature according to  $a + b/(T - T_0)$  where  $a, b$

are constants. Then, for a fixed charge to mass ratio we observed an infinite change of slope at  $T = T_0$  signaling a second order phase transition. As we increase the charge the temperature dependence changes drastically.

The paper is organized as follows. In section 2 we review the basic properties of the topological black holes and we discuss their thermodynamics. In section 3 we present the analytical calculations of the QNMs of electromagnetic and gravitational perturbations of the CTBH. In section 4 we study numerically their behaviour and in section 5 we discuss in detail the purely dissipative modes appearing in the spectrum. Finally, section 6 contains our summary.

## 2 Thermodynamics

We consider the action

$$I = \int d^4x \sqrt{-g} \left[ \frac{R + 6l^{-2}}{16\pi G} \right],$$

where  $l$  is the AdS radius. The presence of a negative cosmological constant ( $\Lambda = -3l^{-2}$ ) allows the existence of black holes with a topology  $R^2 \times \Sigma$ , where  $\Sigma$  is a two-dimensional manifold of constant curvature. These black holes are known as topological black holes [16]-[20]. The simplest solution of this kind, when  $\Sigma$  has negative constant curvature, reads

$$ds^2 = - \left( -1 + \frac{r^2}{l^2} - \frac{2G\mu}{r} \right) dt^2 + \frac{dr^2}{\left( -1 + \frac{r^2}{l^2} - \frac{2G\mu}{r} \right)} + r^2 d\sigma^2, \quad (2.1)$$

where  $d\sigma^2$  is the line element of  $\Sigma$ , which is locally isomorphic to the hyperbolic manifold  $H^2$  and  $\Sigma$  must be of the form

$$\Sigma = H^2/\Gamma \quad \text{with} \quad \Gamma \subset O(2,1),$$

where  $\Gamma$  is a freely acting discrete subgroup (i.e., without fixed points).

The configurations (2.1) are asymptotically locally AdS spacetimes. It has been shown in [21] that the massless configurations where  $\Sigma$  has negative constant curvature are stable under gravitational perturbations. More recently the stability of the topological black holes was discussed in [22].

If we introduce to the above action an electromagnetic field

$$-\frac{1}{16\pi} \int d^4x \sqrt{-g} F^{\mu\nu} F_{\mu\nu}$$

then the metric of a charged topological black hole is given by

$$ds^2 = -f(r)dt^2 + \frac{dr^2}{f(r)} + r^2 d\sigma^2, \quad f(r) = r^2 - 1 - \frac{2G\mu}{r} + \frac{q^2}{r^2}, \quad (2.2)$$

where we have fixed the length of the AdS space to  $l = 1$ . The horizon  $r_+$  is specified from

$$q^2 = 2G\mu r_+ + r_+^2 - r_+^4. \quad (2.3)$$

Define the charge to mass ratio by

$$\frac{q^2}{(G\mu)^2} = \lambda^2 . \quad (2.4)$$

Then using (2.3) we have<sup>1</sup>

$$G\mu = \frac{r_+(r_+^2 - 1)}{1 + \sqrt{1 - \lambda^2(r_+^2 - 1)}} . \quad (2.5)$$

We consider an electric potential at the horizon  $\Phi = -q/r_+$  and the electric charge  $Q = \sigma q/4\pi$ . The temperature, the entropy and the mass of the CTBH are given by

$$\begin{aligned} T &= \frac{f'(r_+)}{4\pi} = \frac{3r_+^4 - r_+^2 - q^2}{4\pi r_+^3} , \\ S &= \frac{\sigma r_+^2}{4G} , \\ M &= \frac{\sigma\mu}{4\pi} = \frac{\sigma(r_+^4 - r_+^2 + q^2)}{8\pi G r_+} . \end{aligned} \quad (2.6)$$

With the help of

$$dM = \frac{\sigma(3r_+^2 - 1 - \frac{Gq^2}{r_+^2})}{8\pi G} dr_+ + \frac{\sigma q}{4\pi r_+} dq$$

it is easy to verify that the law of thermodynamics

$$dM = TdS - \Phi dQ \quad (2.7)$$

is valid. The free energy is

$$F = M - TS + Q\Phi = -\frac{\sigma(r_+^3 + r_+)}{16\pi G} - \frac{\sigma q^2}{16\pi r_+} = -\frac{\sigma}{16\pi G} \left[ r_+^3 + r_+ + \frac{\lambda^2(G\mu)^2}{r_+} \right] , \quad (2.8)$$

where  $G\mu$  should be replaced by its value in eq. (2.5) and then

$$dF = -SdT + Qd\Phi \quad (2.9)$$

is easily verified. Notice now that the critical temperature

$$T_0 = \frac{1}{2\pi} \quad (2.10)$$

---

<sup>1</sup>There is another possibility,

$$G\mu = \frac{r_+(r_+^2 - 1)}{1 - \sqrt{1 - \lambda^2(r_+^2 - 1)}}$$

We shall not discuss it here because it corresponds to configurations which do not approach the critical point  $r_+ = 1$ .

corresponds to  $r_+ = 1$ . We have already given the functions  $F(r_+)$  and  $T(r_+)$ , so we can readily Taylor expand  $F(T)$  about  $T_0$  and express the necessary derivatives through the formulae

$$\frac{dF}{dT} = \frac{F'}{T'}, \quad \frac{d^2F}{dT^2} = \frac{T'F'' - F'T''}{T'^3}, \quad \frac{d^3F}{dT^3} = \frac{3F'T''^2 + T'^2F^{(3)} - 3T'T''F'' - F'T'T^{(3)}}{T'^5}, \dots,$$

where primes denote differentiations with respect to  $r_+$ . The expansion of the free energy finally reads:

$$\begin{aligned} F &= -\frac{\sigma}{8\pi G} \left( 1 + 2(T - T_0)\pi + (2 + \lambda^2)(T - T_0)^2\pi^2 \right. \\ &\quad \left. + \frac{(2 + 3\lambda^2)(1 + \lambda^2)}{2}(T - T_0)^3\pi^3 + \dots \right). \end{aligned} \quad (2.11)$$

It is interesting to consider how formulae (2.3) - (2.11) simplify in two important special cases, namely when  $\lambda^2$  takes on the values  $-1$  or  $0$ . Notice that having chosen a definite value for  $\lambda$  means that  $q$  and  $r_+$  are no longer independent.

(a)  $\lambda^2 = -1$  (CTBH with scalar hair [28])

$$ds^2 = -f(r)dt^2 + \frac{dr^2}{f(r)} + r^2d\sigma^2, \quad f(r) = r^2 - \left(1 + \frac{G\mu}{r}\right)^2. \quad (2.12)$$

The horizon  $r_+$  is specified from

$$G\mu = r_+(r_+ - 1), \quad (2.13)$$

and the relevant quantities become

$$Q = \frac{\sigma q}{4\pi} \quad (2.14)$$

$$\begin{aligned} T &= \frac{f'(r_+)}{4\pi} = \frac{2r_+ - 1}{2\pi}, \\ S &= \frac{\sigma r_+^2}{4G} \Rightarrow dS = \frac{\sigma r_+ dr_+}{2G}, \\ M &= \frac{\sigma\mu}{4\pi} = \frac{\sigma(r_+^2 - r_+)}{4\pi G}. \end{aligned} \quad (2.15)$$

$$dM = TdS - \Phi dQ, \quad (2.16)$$

$$F = M - TS + Q\Phi = -\frac{\sigma r_+^2}{8\pi G}, \quad (2.17)$$

$$dF = -SdT + Qd\Phi, \quad (2.18)$$

$$F = -\frac{\sigma}{8\pi G} \left( 1 + 2(T - T_0)\pi + (T - T_0)^2\pi^2 + O(T - T_0)^4 \right).$$

(b)  $\lambda^2 = 0$  (Uncharged topological black hole) with

$$f(r) = r^2 - 1 - \frac{2G\mu}{r}, \quad (2.19)$$

$$2G\mu = r_+^3 - r_+ , \quad (2.20)$$

$$Q = \sigma q/4\pi = 0 . \quad (2.21)$$

$$\begin{aligned} T &= \frac{f'(r_+)}{4\pi} = \frac{3r_+^2 - 1}{4\pi r_+} , \\ S &= \frac{\sigma r_+^2}{4G} \Rightarrow dS = \frac{\sigma r_+ dr_+}{2G} , \\ M &= \frac{\sigma\mu}{4\pi} = \frac{\sigma(r_+^3 - r_+)}{8\pi G} \Rightarrow dM = \frac{\sigma(3r_+^2 - 1)}{8\pi G} dr_+ . \end{aligned} \quad (2.22)$$

$$dM = TdS , \quad (2.23)$$

$$F = M - TS = -\frac{\sigma(r_+^3 + r_+)}{16\pi G} , \quad (2.24)$$

$$dF = -SdT , \quad (2.25)$$

$$F = -\frac{\sigma}{8\pi G} \left( 1 + 2(T - T_0)\pi + 2(T - T_0)^2\pi^2 + (T - T_0)^3\pi^3 + \dots \right) . \quad (2.26)$$

As an application of the above considerations if we assume that

$$f(r) = r^2 - \left( 1 + \frac{G\mu}{r} \right)^2 \quad (2.27)$$

solves a four dimensional gravitational action describing a gravitational field coupled to a scalar and to an EM field (charged MTZ black hole [28]), calculating the quantity

$$F_{CTBH} - F_{CMTZ} = -\frac{\pi^2\sigma(2 + 3\lambda^2)(1 + \lambda^2)}{16G} (T - T_0)^3\pi^3 + \dots \quad (2.28)$$

we see that it is changing sign as we cross the critical temperature, hence we have a phase transition of the charged MTZ black hole to CTBH.

### 3 Gravitational and Electromagnetic Modes

The radial wave equation for gravitational perturbations in the black-hole background can be cast into a Schrödinger-like form [29],

$$-\frac{d^2\Psi}{dr_*^2} + V[r(r_*)]\Psi = \omega^2\Psi , \quad (3.1)$$

in terms of the tortoise coordinate defined by

$$\frac{dr_*}{dr} = \frac{1}{f(r)} . \quad (3.2)$$

The potential  $V$  is determined by the type of perturbation. For axial perturbations, we have

$$V(r) = V_A^\pm(r) \equiv f(r) \left\{ \frac{\Lambda}{r^2} - \frac{3G\mu[1 \pm \Delta]}{r^3} + \frac{4q^2}{r^4} \right\} , \quad (3.3)$$

where

$$\Delta = \sqrt{1 + \frac{4}{9}(\Lambda + 2)\lambda^2} , \quad (3.4)$$

and  $\Lambda$  are the eigenvalues resulting from the the solution of Laplace-Beltrami equation  $\Delta\psi = -\Lambda\psi$  on a space which has constant negative curvature and which is of the form  $P_{-\frac{1}{2} \pm i\xi}^m(\cosh r)e^{im\phi}(\cosh r)$  and the corresponding eigenvalues read:  $\Lambda = -l(l + 1)$  with  $l = -\frac{1}{2} \pm i\xi$ , so that  $\Lambda = \frac{1}{4} + \xi^2$ .

For polar perturbations we have,

$$V(r) = V_P^\pm(r) \equiv \frac{f(r)U_\pm(r)}{r^2(\Lambda + 2 + 3(1 \pm \Delta)\frac{G\mu}{r})^2} , \quad (3.5)$$

where

$$\begin{aligned} U_\pm(r) = & 18(1 \pm \Delta)^2 G^2 \mu^2 + \frac{81}{2} \frac{1 - \Delta^2}{\Lambda + 2} (1 \pm \Delta)^2 \frac{G^4 \mu^4}{r^4} + 9(1 \pm \Delta)^2 (5 \mp 3\Delta) \frac{G^3 \mu^3}{r^3} \\ & + 18(1 \pm \Delta)(\Lambda + 2) \frac{G^2 \mu^2}{r^2} + 3(\Lambda + 2)^2 (1 \pm \Delta) \frac{G\mu}{r} + \Lambda(\Lambda + 2)^2 . \end{aligned} \quad (3.6)$$

We shall refer to the modes corresponding to the potential  $V^-$  (axial or polar) as  $Z_1$  modes whereas those corresponding to  $V^+$  will be referred to as  $Z_2$  modes.

The potential for polar perturbations (3.5) has a singularity at

$$r = r_0 = -\frac{3(1 \pm \Delta)G\mu}{\Lambda + 2} \quad (3.7)$$

in addition to the standard singularities  $r = r_+, \infty$ . Remarkably, at the singularity (3.7),

$$U_\pm(r_0) = 2(\Lambda + 2)^2 f(r_0) , \quad (3.8)$$

resulting in the behaviour of the wavefunction

$$\Psi \sim (r - r_0)^\alpha , \quad \alpha = 2, -1 . \quad (3.9)$$

It turns out that at the boundary ( $r \rightarrow \infty$ ), the wavefunction has the same behavior with  $\alpha = -1$ . Precisely,

$$\Psi \sim (1 - r_0/r)^{-1} \quad (3.10)$$

so it does not obey the Dirichlet boundary condition  $\Psi = 0$ . Instead, it obeys the *Robin* boundary condition [30, 31]

$$r^2 \Psi' + r_0 \Psi = 0 \quad (r \rightarrow \infty) . \quad (3.11)$$



This is true even in the limit  $q = 0$  for the  $Z_2$  mode. For the  $Z_1$  mode,  $r_0 = 0$  if  $q = 0$ , so we obtain the standard  $\Psi \rightarrow 0$  boundary condition. The latter is the electromagnetic mode. Indeed, if  $q = 0$ ,  $\Delta = 1$ , so

$$U_-(r) = (\Lambda + 2)^2 \Lambda , \quad V_-(r) = \Lambda \frac{f(r)}{r^2} . \quad (3.12)$$

Evidently, the potential vanishes at the horizon ( $V(r_+) = 0$ , since  $f(r_+) = 0$ ). This is the case for all types of perturbation.

To obtain analytic expressions for the quasi-normal frequencies, it is convenient to introduce the coordinate [31]

$$u = \frac{r_+}{r} . \quad (3.13)$$

The wave equation (3.1) becomes

$$(u^2 \hat{f}(u) \Psi')' + \left[ \frac{\hat{\omega}^2}{u^2 \hat{f}(u)} - \frac{\hat{V}}{u^2 \hat{f}} \right] \Psi = 0 , \quad \hat{\omega} = \frac{\omega}{r_+} , \quad (3.14)$$

where prime denotes differentiation with respect to  $u$  and we have defined

$$\hat{f}(u) \equiv \frac{f(r)}{r_+^2} = \frac{1}{u^2} - \frac{1}{r_+^2} - \frac{2G\mu}{r_+^3} u + \frac{q^2}{r_+^4} u^2 , \quad \hat{V}(u) \equiv \frac{V(r)}{r_+} . \quad (3.15)$$

For the various potentials, we obtain

$$\hat{V}_A^\pm(u) = \hat{f}(u) \left\{ \hat{\Lambda} u^2 - \frac{3G\mu[1 \pm \Delta]}{r_+^3} u^3 + \frac{4q^2}{r_+^4} u^4 \right\} , \quad \hat{\Lambda} = \frac{\Lambda}{r_+^2} \quad (3.16)$$

and

$$\hat{V}_P^\pm(u) = \frac{u^2 \hat{f}(u) \hat{U}_\pm(u)}{(\tilde{\Lambda} + 3(1 \pm \Delta) \frac{G\mu}{r_+^3} u)^2} , \quad (3.17)$$

$$\begin{aligned} \hat{U}_\pm(u) &\equiv \frac{U_\pm(r)}{r_+^6} \\ &= 18(1 \pm \Delta)^2 \frac{G^2 \mu^2}{r_+^6} + \frac{81}{2} \frac{1 - \Delta^2}{\tilde{\Lambda}} (1 \pm \Delta)^2 \frac{G^4 \mu^4}{r_+^{12}} u^4 + 9(1 \pm \Delta)^2 (5 \mp 3\Delta) \frac{G^3 \mu^3}{r_+^9} u^3 \\ &\quad + 18(1 \pm \Delta) \tilde{\Lambda} \frac{G^2 \mu^2}{r_+^6} u^2 + 3\tilde{\Lambda}^2 (1 \pm \Delta) \frac{G\mu}{r_+^3} u + \tilde{\Lambda}^3 - 2\tilde{\Lambda}^2 \frac{1}{r_+^2} , \end{aligned} \quad (3.18)$$

where

$$\tilde{\Lambda} = \hat{\Lambda} + \frac{2}{r_+^2} . \quad (3.19)$$

### 3.1 QNMs of Large Black Holes

To study the form of quasi-normal modes for large horizons, it is convenient to factor out the behaviour of the wavefunction at the horizon ( $u = 1$ ),

$$\Psi = (1 - u)^{-i\frac{\omega}{4\pi T_H}} F(u) . \quad (3.20)$$

The wave equation becomes

$$\mathcal{A}_{r_+} F'' + \mathcal{B}_{r_+, \hat{\omega}} F' + \mathcal{C}_{\hat{\omega}, \hat{\Lambda}} F = 0 , \quad (3.21)$$

where

$$\begin{aligned} \mathcal{A}_{r_+} &= u^2 \hat{f} , \\ \mathcal{B}_{r_+, \hat{\omega}} &= (u^2 \hat{f})' + 2 \frac{i\omega}{4\pi T_H} \frac{u^2 \hat{f}}{1 - u} , \\ \mathcal{C}_{\hat{\omega}, \hat{\Lambda}} &= \frac{\hat{\omega}^2}{u^2 \hat{f}} - \frac{\hat{V}}{u^2 \hat{f}} - \frac{\omega^2}{(4\pi T_H)^2} \frac{u^2 \hat{f}}{(1 - u)^2} + \frac{i\omega}{4\pi T_H} \frac{(u^2 \hat{f})'}{1 - u} + \frac{i\omega}{4\pi T_H} \frac{u^2 \hat{f}}{(1 - u)^2} . \end{aligned} \quad (3.22)$$

For  $V = V_{\Lambda}^+$  (axial  $Z_2$  modes), this wave equation may be solved for small  $\hat{\omega}$ ,  $\hat{\Lambda}$ . To employ perturbation theory, write eq. (3.21) as

$$(\mathcal{H}_0 + \mathcal{H}_1)F = 0 , \quad (3.23)$$

where

$$\begin{aligned} \mathcal{H}_0 F &\equiv \mathcal{A}_{\infty} F'' + \mathcal{B}_{\infty, 0} F' + \mathcal{C}_{0, 0} F , \\ \mathcal{H}_1 F &\equiv (\mathcal{A}_{r_+} - \mathcal{A}_{\infty}) F'' + (\mathcal{B}_{r_+, \hat{\omega}} - \mathcal{B}_{\infty, 0}) F' + (\mathcal{C}_{\hat{\omega}, \hat{\Lambda}} - \mathcal{C}_{0, 0}) F . \end{aligned} \quad (3.24)$$

The zeroth order equation  $\mathcal{H}_0 F_0 = 0$  is obtained by letting  $\hat{\omega}$ ,  $\hat{\Lambda} \rightarrow 0$ ,  $r_+ \rightarrow \infty$  while keeping  $G\mu/r_+^3$  and  $q^2/r_+^4$  fixed. We have  $\Delta \rightarrow 1$ , so

$$(u^2 \hat{f}_0(u) F_0')' - \left[ -\frac{6G\mu}{r_+^3} u + \frac{4q^2}{r_+^4} u^2 \right] F_0 = 0 . \quad (3.25)$$

Despite its apparent complexity, the acceptable solution takes a remarkably simple form,

$$F_0(u) = u . \quad (3.26)$$

The first-order constraint reads

$$\int_0^1 F_0 \mathcal{H}_1 F_0 = 0 , \quad (3.27)$$

which imposes a constraint on the parameters (dispersion relation) of the form

$$\mathbf{a}_0 - i\mathbf{a}_1 \hat{\omega} - \mathbf{a}_2 \hat{\omega}^2 = 0 . \quad (3.28)$$

After some algebra, we arrive at explicit expressions for the coefficients,

$$\begin{aligned} \mathbf{a}_0 &= -\int_0^1 u^2 \left[ -\hat{\Lambda} - \frac{2}{r_+^2} + \frac{3G\mu(\Delta-1)}{r_+^3} u \right] = \frac{\hat{\Lambda} + \frac{2}{r_+^2}}{3} + \frac{3G\mu(1-\Delta)}{4}, \\ \mathbf{a}_1 &= -\frac{r_+}{4\pi T_H} \int_0^1 u^2 \left[ \frac{2u\hat{f}_0}{1-u} + \left( \frac{u^2\hat{f}_0}{1-u} \right)' \right] = -\frac{r_+}{4\pi T_H} \left( \frac{u^4\hat{f}_0}{1-u} \right) \Big|_0^1 = 1. \end{aligned} \quad (3.29)$$

The other coefficient,  $\mathbf{a}_2$  is not needed for the lowest mode. Therefore,

$$i\hat{\omega} = \mathbf{a}_0 = \frac{\hat{\Lambda} + \frac{2}{r_+^2}}{3} + \frac{3G\mu(1-\Delta)}{4r_+^3}. \quad (3.30)$$

Explicitly, for large  $r_+$ ,

$$\omega = -i \frac{(\Lambda+2)r_+^2}{6G\mu}, \quad (3.31)$$

which is a purely dissipative mode. Notice that  $\omega \propto 1/r_+$ , because  $G\mu \propto r_+^3$  for large  $r_+$ .

For  $Z_1$  axial perturbations ( $V = V_A^-$ ), there is no solution in the small  $\hat{\omega}$  limit. This indicates that the lowest lying modes are proportional to  $r_+$  (so that  $\hat{\omega} = \omega/r_+$  remains finite as  $r_+ \rightarrow \infty$ ). Explicit analytic expressions cannot be obtained in general. However, as we discuss later, in the case of  $q = 0$  the wavefunction may be written in terms of a Heun function leading to semi-analytic expressions for the frequencies.

The calculation of polar modes is considerably more involved due to the additional singularity of the potential [31]. The spectrum is similar to the spectrum of axial modes as evidenced by our numerical calculations (section 4). We shall not perform the analytical calculation of these modes for large black holes as our main focus is on the critical point ( $r_+ = 1$ ) to which we turn next.

### 3.2 QNMs at the Critical Point

At the critical point ( $r_+ = 1, q = 0, \mu = 0$ ), the wave equation for all types of perturbations reduces to

$$((1-u^2)\Psi')' + \left[ \frac{\omega^2}{1-u^2} - \Lambda \right] \Psi = 0, \quad (3.32)$$

whose solutions can be written in terms of associated Legendre functions. The solution which is well-behaved at the horizon is

$$\Psi(u) = P_{i\xi-1/2}^{i\omega}(u). \quad (3.33)$$

To see that it is regular at  $u = 1$ , express it in terms of a hypergeometric function,

$$\Psi(u) = \frac{1}{\Gamma(1-i\omega)} \left( \frac{1+u}{1-u} \right)^{i\omega/2} F\left(-i\xi + \frac{1}{2}, i\xi + \frac{1}{2}; 1-i\omega; \frac{1-u}{2}\right). \quad (3.34)$$

At the boundary,  $u \rightarrow 0$ , it approaches a constant,

$$\Psi(0) = P_{i\xi-1/2}^{i\omega}(0) = \frac{2^{i\omega} \sqrt{\pi}}{\Gamma\left(\frac{3}{4} - \frac{1}{2}i\xi - \frac{1}{2}i\omega\right) \Gamma\left(\frac{3}{4} + \frac{1}{2}i\xi - \frac{1}{2}i\omega\right)}. \quad (3.35)$$

Demanding that it vanish, we deduce the quasi-normal frequencies

$$\omega_n = \pm\xi - i\left(2n + \frac{3}{2}\right) \quad , \quad n = 0, 1, 2, \dots \quad (3.36)$$

which have finite real part (except in the special case  $\xi = 0$ ).

For explicit expressions, use

$$F(\alpha, \beta; \gamma; z) = (1-z)^{\gamma-\alpha-\beta} F(\gamma-\alpha, \gamma-\beta; \gamma; z)$$

to write

$$\Psi_n(u) = A_n(1-u^2)^{-i\omega_n/2} F(-i\omega_n + i\xi + \frac{1}{2}, -i\omega_n - i\xi + \frac{1}{2}; 1 - i\omega_n; \frac{1-u}{2}) \quad . \quad (3.37)$$

These hypergeometric functions are polynomials. Explicitly,

$$\begin{aligned} \Psi_0(u) &= A_0(1-u^2)^{-i\xi/2-3/4} u \quad , \\ \Psi_1(u) &= A_1(1-u^2)^{-i\xi/2-7/4} u \left[ 1 + \frac{2+2i\xi}{3} u^2 \right] \quad , \end{aligned} \quad (3.38)$$

etc. They are orthogonal under the inner product (no complex conjugation!)

$$\langle n|m \rangle \equiv \int_0^1 \frac{du}{1-u^2} \Psi_n(u) \Psi_m(u) \quad (3.39)$$

defined by appropriate analytic continuation of the parameter  $\xi$ . To normalize them ( $\langle n|n \rangle = 1$ ), choose

$$A_0^2 = \frac{4\Gamma(-i\xi)}{\sqrt{\pi}\Gamma(-i\xi - \frac{3}{2})} \quad , \quad A_1^2 = \frac{6\Gamma(-i\xi - 1)}{\sqrt{\pi}(-i\xi - \frac{5}{2})\Gamma(-i\xi - \frac{7}{2})} \quad , \quad (3.40)$$

etc.

Moving away from the critical point, the frequencies shift by

$$\delta\omega_n = \frac{1}{2\omega_n} \frac{\langle n|\mathcal{H}'|n \rangle}{\langle n|n \rangle} \quad , \quad (3.41)$$

where

$$\mathcal{H}'\Psi_n = -u^2 \hat{f}(u) \left( u^2 \hat{f}(u) \Psi_n' \right)' + \hat{V}(u) \Psi_n - \omega^2 \Psi_n \quad , \quad (3.42)$$

where we applied standard first-order perturbation theory.

We obtain for the axial modes

$$\begin{aligned} \delta\omega_0 &= i \left( 1 - \frac{1}{r_+^2} \right) \left[ \frac{3}{2} + i\xi + \left( \frac{3(1 \pm \Delta)}{4} + i\xi \right) \frac{4\Gamma(-i\xi)}{\sqrt{\pi}\Gamma(\frac{3}{2} - i\xi)} \right] \quad , \\ \delta\omega_1 &= i \left( 1 - \frac{1}{r_+^2} \right) \left[ \frac{7}{2} + i\xi - \frac{\left\{ \frac{27}{4}(1 \pm \Delta) - 2 + 9 \left( 1 + \frac{1 \pm \Delta}{2} \right) i\xi - 14\xi^2 \right\} \Gamma(-1 - i\xi)}{\sqrt{\pi}\Gamma(\frac{3}{2} - i\xi)} \right] \quad . \end{aligned} \quad (3.43)$$

For small  $\xi$ , the change in the imaginary part is negligible whereas the change in the real part is

$$\delta\omega_0 \approx - \left(1 - \frac{1}{r_+^2}\right) \frac{3(1 \pm \Delta)}{2\pi\xi} . \quad (3.44)$$

For  $Z_2$  modes, above the critical point ( $r_+ > 1$ ),  $\delta\omega_0 < 0$  and the real part decreases. There is a critical value of  $\xi$  (determined by  $\xi + \delta\omega_0 \approx 0$ ),

$$\xi_0 \approx \sqrt{12(1 + \Delta)(T - T_0)} , \quad (3.45)$$

where we used  $T - T_0 \approx \frac{1}{4\pi} \left(1 - \frac{1}{r_+^2}\right)$ , below which the mode does not propagate (purely dissipative mode). It turns out that for  $\xi < \xi_0$  there is a pair of purely dissipative modes.

The first harmonic behaves similarly with a higher critical value of  $\xi$ ,

$$\xi_1 \approx \sqrt{[27(1 + \Delta) - 8](T - T_0)} \quad (3.46)$$

below which it turns into a pair of purely dissipative modes.

Below the critical point ( $r_+ < 1$ ),  $\delta\omega_0 > 0$  and the real part of the  $Z_2$  modes increases. The modes do not become purely dissipative for any value of  $\xi$ .

Also notice that above the critical point,  $\delta\omega_n$  increases with  $n$ , therefore the real part decreases with  $n$  (positive slope) whereas below the critical point we obtain a *negative* slope for propagating modes.

$Z_1$  modes behave in the opposite way because  $1 - \Delta < 0$ . Above the critical point, these modes never become purely dissipative. Below the critical point, we obtain the critical values

$$\xi_0 \approx \sqrt{12(\Delta - 1)(T - T_0)} , \quad \xi_1 \approx \sqrt{[8 + 27(\Delta - 1)](T - T_0)} \quad (3.47)$$

similar to  $Z_2$  modes above the critical point.

For the polar modes we obtain

$$\begin{aligned} \delta\omega_0 &= i \left(1 - \frac{1}{r_+^2}\right) \left[ \frac{3}{2} + i\xi + \left(3(1 \pm \Delta) \frac{\Lambda - 2}{\Lambda + 2} + i\xi\right) \frac{4\Gamma(-i\xi)}{\sqrt{\pi}\Gamma(\frac{3}{2} - i\xi)} \right] , \\ \delta\omega_1 &= i \left(1 - \frac{1}{r_+^2}\right) \left[ \frac{7}{2} + i\xi - \frac{\left\{ -\frac{9}{2}(1 \pm \Delta) \frac{\Lambda + \frac{3}{2}}{\Lambda + 2} \left(\frac{3}{2} + i\xi\right) - 2 + 9i\xi - 14\xi^2 \right\} \Gamma(-1 - i\xi)}{\sqrt{\pi}\Gamma(\frac{3}{2} - i\xi)} \right] . \end{aligned} \quad (3.48)$$

These modes coincide with their axial counterparts for  $\Delta = -1$  (electromagnetic modes).

### 3.3 Uncharged Black Holes

In the case of no charge in the black hole, the wave equations simplify because  $u^2 \hat{f}(u)$  has at most three distinct roots,  $u = 1, \eta, -\frac{\eta}{1+\eta}$ , where

$$\eta = - \frac{2}{1 + \sqrt{1 - 4(1 - 1/r_+^2)}} . \quad (3.49)$$

Then the solution to the wave equation may be written in terms of a Heun function.

For  $Z_1$  perturbations, the potentials for axial and polar modes coincide reducing to the electromagnetic potential. The wavefunction may be written as

$$\begin{aligned} \Psi(u) &= (u - \eta)^{-i\hat{\omega}\frac{\eta}{(1-\eta)(2+\eta)}} \left( u + \frac{\eta}{1+\eta} \right)^{i\hat{\omega}\frac{\eta(1+\eta)}{(2+\eta)(1+2\eta)}} (1-u)^{i\hat{\omega}\frac{\eta^2}{(1-\eta)(1+2\eta)}} \\ &\times \text{Heun}(a, q, \alpha, \beta, \gamma, \delta, \frac{1-u}{1-\eta}) . \end{aligned} \quad (3.50)$$

The Heun function obeys the equation

$$z(z-1)(z-a)F'' - [(-\alpha-\beta-1)z^2 + ((\delta+\gamma)a - \delta + \alpha + \beta + 1)z - a\gamma]F' - [-\alpha\beta z + q]F = 0 \quad (3.51)$$

and the various constants are

$$\begin{aligned} a &= \frac{1+2\eta}{1-\eta^2} , & q &= -\Lambda \frac{1+\eta+\eta^2}{1-\eta^2} , \\ \alpha &= 0 , & \beta &= 2 , & \gamma &= \frac{1+\eta-2(1-i\hat{\omega})\eta^2}{(1-\eta)(1+2\eta)} , & \delta &= \frac{2-(2i\hat{\omega}+1)\eta-\eta^2}{(1-\eta)(2+\eta)} . \end{aligned}$$

It behaves nicely at the horizon ( $u \rightarrow 1$ ). Requiring  $\Psi(0) = 0$  yields the constraint

$$\text{Heun}(a, q, \alpha, \beta, \gamma, \delta, \frac{1}{1-\eta}) = 0 , \quad (3.52)$$

which may be solved for  $\hat{\omega}$  to obtain the quasi-normal frequencies of axial  $Z_1$  modes.

As  $r_+ \rightarrow \infty$ , the two lowest purely dissipative modes asymptote respectively to

$$\omega_0 = -i\frac{3}{2}r_+ , \quad \omega_1 = -3ir_+ \quad (3.53)$$

if  $\Lambda$  is kept constant. As  $\Lambda$  increases, the two modes approach each other coalescing at

$$\Lambda = 0.115r_+^2 , \quad \omega_0 = \omega_1 = -2.05ir_+ \quad (3.54)$$

Beyond this point, they develop a finite real part.

For axial  $Z_2$  perturbations, the solution to the wave equation may be similarly written as

$$\begin{aligned} \Psi(u) &= (u - \eta)^{-i\hat{\omega}\frac{\eta}{(1-\eta)(2+\eta)}} \left( u + \frac{\eta}{1+\eta} \right)^{i\hat{\omega}\frac{\eta(1+\eta)}{(2+\eta)(1+2\eta)}} (1-u)^{i\hat{\omega}\frac{\eta^2}{(1-\eta)(1+2\eta)}} \\ &\times \text{Heun}(a, q', \alpha', \beta', \gamma, \delta, \frac{1-u}{1-\eta}) , \end{aligned} \quad (3.55)$$

where the parameters  $a, \gamma, \delta$  are same as before and

$$q' = -\frac{(1+\eta+\eta^2)\Lambda + 3(1+\eta)}{1-\eta^2} , \quad \alpha' = -1 , \quad \beta' = 3 . \quad (3.56)$$

It behaves nicely at the horizon ( $u \rightarrow 1$ ). Requiring  $\Psi(0) = 0$  yields the constraint

$$\text{Heun}(a, q', \alpha', \beta', \gamma, \delta, \frac{1}{1-\eta}) = 0, \quad (3.57)$$

which may be solved for  $\hat{\omega}$  to obtain the quasi-normal frequencies of axial  $Z_2$  modes.

As  $r_+ \rightarrow \infty$ , we find a single purely dissipative axial  $Z_2$  mode which asymptotes to

$$\omega_0 = -i \frac{\Lambda + 2}{3r_+} \quad (3.58)$$

confirming the earlier analytical result (3.31) in the case  $q = 0$ .

The above results do not apply to polar  $Z_2$  perturbations due to the additional singularity in the potential which survives the limit  $q \rightarrow 0$ .

## 4 Numerical Calculations and Results

We briefly review the method of Horowitz and Hubeny [4] as it is applied to our problem. After performing the transformation  $\Psi(r) = \psi_\omega(r)e^{-i\omega r^*}$ , the wave equation (3.1) becomes

$$f(r) \frac{d^2 \psi_\omega(r)}{dr^2} + \left( \frac{df(r)}{dr} - 2i\omega \right) \frac{d\psi_\omega(r)}{dr} = V(r)\psi_\omega(r), \quad (4.1)$$

where the potential  $V(r)$  is given by (3.16) or (3.17). The change of variables  $r = 1/x$  yields an equation of the form

$$s(x) \left[ (x - x_+)^2 \frac{d^2 \psi_\omega(x)}{dx^2} \right] + t(x) \left[ (x - x_+) \frac{d\psi_\omega(x)}{dx} \right] + u(x)\psi_\omega(x) = 0,$$

where  $x_+ = 1/r_+$  and  $s(x), t(x)$  and  $u(x)$  are given by

$$\begin{aligned} s(x) &= \sum_{n=0}^k s_n (x - x_+)^k, \\ t(x) &= \sum_{n=0}^k t_n (x - x_+)^k, \\ u(x) &= \sum_{n=0}^k u_n (x - x_+)^k, \end{aligned}$$

where  $k = 3$  for axial and  $k = 7$  for polar perturbations. Expanding the wavefunction around the (inverse) horizon  $x_+$ ,

$$\psi_\omega(x) = \sum_0^\infty a_n(\omega)(x - x_+)^n, \quad (4.2)$$

we arrive at a recurrence formula for the coefficients,

$$a_n(\omega) = -\frac{1}{n(n-1)s_0 + nt_0 + u_0} \sum_{m=n-3}^{n-1} [m(m-1)s_{n-m} + mt_{n-m} + u_{n-m}]a_m(\omega). \quad (4.3)$$

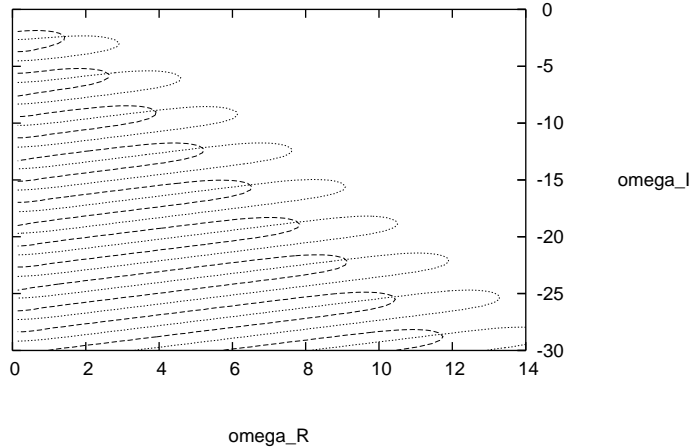


Figure 1: QNMs of axial  $Z_1$  perturbations with  $r_+ = 1.50$ ,  $\nu = 0.10$ .

We note that the few coefficients  $a_m(\omega)$  with negative index  $m$  which will appear for  $n < 2$  should be set to zero, while  $a_0(\omega)$  is set to one. Since the wave function should vanish at infinity ( $r \rightarrow \infty, x = 0$ ), we deduce

$$\psi_\omega(0) \equiv \sum_0^\infty a_n(\omega)(-x_+)^n = 0 . \quad (4.4)$$

The solutions of this equation are precisely the quasi-normal frequencies.

### 4.1 Overview and Spacing

To begin with, let us recall the expression for the temperature given earlier:  $T = \frac{3r_+^4 - r_+^2 - q^2}{4\pi r_+^3}$ . The constraint that  $T$  should be positive yields the inequality  $q^2 \leq q_{max}^2 \equiv 3r_+^4 - r_+^2$ , so the charge may be expressed through the parameter

$$\nu \equiv \frac{Q}{Q_{max}} , \quad Q_{max} = \frac{\sigma}{4\pi} \sqrt{3r_+^4 - r_+^2} . \quad (4.5)$$

We note that this parameter is related to the charge-to-mass ratio  $\lambda$  through the equation

$$\lambda^2 = \frac{4\nu^2(3r_+^2 - 1)}{(3\nu^2 r_+^2 + r_+^2 - \nu^2 - 1)^2} .$$

One needs to examine separately large ( $r_+ > 1$ ) and small ( $r_+ < 1$ ) horizons. A typical graph for axial perturbations at  $r_+ = 1.50, \nu = 0.10$  ( $\lambda = 0.37$ ) may be seen in Fig. 1. The figure depicts the curves  $\Re[\psi(\omega)] = 0$  and  $\Im[\psi(\omega)] = 0$  in the complex  $\omega$  plane. The QNMs are given by the intersections of the curves. We remark that, if one views  $\omega_I$  versus  $\omega_R$ , the slope is negative, as can be seen in Fig. 1; this feature does not change if one varies  $\nu$ . This specific graph depicts axial  $Z_1$  QNMs at  $r_+ = 1.50$  and  $\nu = 0.10$ , but no qualitative change occurs if one considers  $Z_2$  rather than  $Z_1$  perturbations. The behaviour



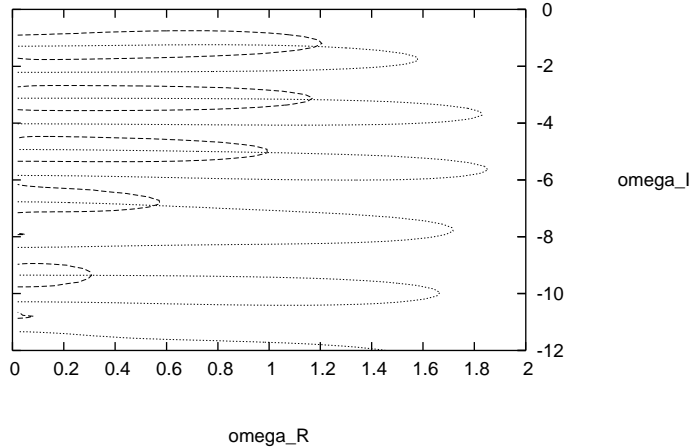


Figure 2: QNMs of axial  $Z_2$  perturbations with  $r_+ = 0.95$ ,  $\nu = 0.10$ .

is similar for polar perturbations: for this value of  $r_+$  only some quantitative changes have been observed between the polar perturbations and their axial counterparts.

However, for the small horizon  $r_+ = 0.95$  the behaviour of QNMs is different. For  $\nu = 0.10$  ( $\lambda = 3.25$ ) and axial  $Z_2$  perturbations (Fig. 2) we find a finite number of propagating QNMs with a positive slope. (We note that there might also exist purely dissipative modes with vanishing real part, which are not clearly visible on such graphs; we will examine them in the next section).

For  $\nu = 0.40$  ( $\lambda = 5.95$ ) the pattern is qualitatively different as can be seen in Fig. 3: a part with positive slope coexists with the negative slope frequencies and the number of QNMs is infinite again. We find similar results for the axial  $Z_1$  perturbations, as well as for the polar  $Z_1$  and  $Z_2$  perturbations.

We may also make some quantitative statements about these modes. The asymptotic spacing between the QNMs may be easily read off from the figures and the results are presented in Table 1. For  $r_+ = 0.95$ , the spacing is not constant; thus we report the difference between the lowest and the second lowest QNMs just to get some feeling for the order of magnitude. An important observation is that positive and negative slope parts coexist for  $r_+ = 0.95$  when  $\nu$  is large enough (Fig. 3), so the results for the imaginary parts refer rather to the absolute value than to values with a well defined sign all the way.

## 4.2 Lowest Modes

For  $r_+ > 1$  the QNMs of the form presented in the previous section may be represented as a multiple of the spacing plus their lowest possible value, referred to as the offset in the literature. It is interesting to examine the behaviour of these lowest modes, in addition to the spacing. The charge is given as a fraction  $\nu$  of its maximal value and notice that we cannot increase the charge parameter  $\nu$  beyond a value about 0.40, due to convergence problems.

$r_+$	$\nu$	type	$Z_1$	$Z_2$
1.50	0.10	axial	$1.25 - 3.25i$	$1.25 - 3.30i$
1.50	0.30	axial	$1.05 - 3.85i$	$1.05 - 3.85i$
1.50	0.00	polar	$1.30 - 3.40i$	$1.36 - 3.30i$
1.50	0.40	polar	$0.94 - 4.20i$	$1.03 - 4.17i$
0.95	0.10	axial	$0.26 + 1.67i$	$0.09 + 2.01i$
0.95	0.40	axial	$0.00 + 1.80i$	$0.17 + 2.20i$
0.95	0.00	polar	$0.32 + 1.80i$	$0.38 + 1.70i$
0.95	0.40	polar	$1.90 + 2.30i$	$1.42 + 2.43i$

Table 1: Spacing of QNMs for various values of the parameters  $r_+$  and  $\nu$  with  $\xi = 1$ .

#### 4.2.1 Axial Perturbations

We examine the intermediate horizon  $r_+ = 1.50$  and a typical large horizon, namely  $r_+ = 20.00$ . It turns out that there are qualitative differences between the two. In Fig. 4 one may see the real parts of the axial  $Z_1$  QNMs for  $r_+ = 20.00$  for large horizons and small values of the charge purely dissipative modes are present, which is not the case for intermediate horizons, such as  $r_+ = 1.50$ . We note that no different behaviour of this kind shows up for  $Z_2$  modes.

In Fig. 5 we depict the absolute real part of the lowest axial modes for  $r_+ = 0.95$ . We observe that, as one increases the charge,  $|\Re\omega|$  for  $Z_2$  modes approaches a constant value, which is presumably also the value for the extremal black holes ( $\nu = 1$ ); on the other hand,  $|\Re\omega|$  for  $Z_1$  modes approaches zero.

The agreement with the analytical result (3.43) is good (improving as we approach the critical point  $r_+ \rightarrow 1$ ). In Figs. 6 and 7, we show plots of the analytical expressions for  $|\Re\omega|$  and  $\Im\omega$ , respectively, for  $Z_1$  and  $Z_2$  axial perturbations for two different values of the horizon just below the critical point ( $r_+ = 0.95$  and  $r_+ = 0.995$ ). The accuracy of the analytical approximation decreases as the charge increases and fails when the first-order correction becomes comparable to the zeroth order approximation (3.36). Naturally, the point of failure increases as we approach the critical point.

#### 4.2.2 Polar Perturbations

Qualitative differences show up for the small value  $r_+ = 0.95$ , so we concentrate on this case. In Fig. 8 we present the real and imaginary parts of the axial and polar perturbations of  $Z_1$  and  $Z_2$ .

For  $Z_2$  polar perturbations the real parts (Fig. 8, left panel) do not have the striking behaviour of the axial perturbations, which are zero above  $\nu = 0.25$ . Similarly the imaginary parts (right panel) decrease with  $\nu$  with no spectacular change at  $\nu = 0.25$ , in contrast with their axial counterparts. Here we also observe the very mild behaviour of the polar QNMs with the charge as compared with the axial perturbations.

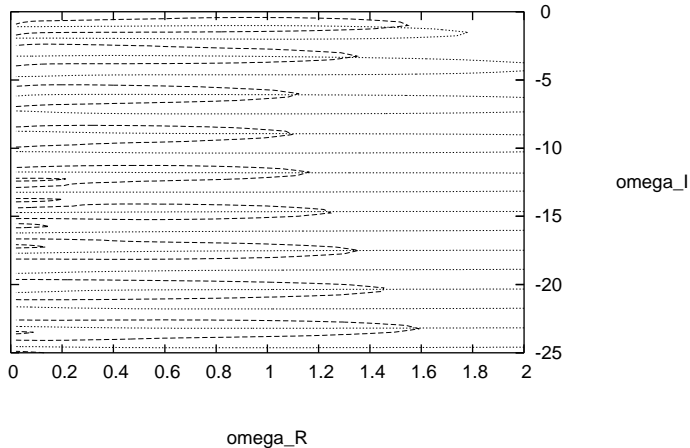


Figure 3: QNMs for axial  $Z_2$  perturbations with  $r_+ = 0.95$ ,  $\nu = 0.40$ .

## 5 Purely Dissipative Modes

After the overview of the propagating QNMs presented in the previous sections, we will make a systematic study of the purely dissipative modes of electromagnetic and gravitational perturbations.

### 5.1 Axial $Z_1$ Modes

Fig. 9 contains the results for purely dissipative QNMs at  $r_+ = 5.00$  and  $r_+ = 1.50$  versus  $\nu$ . For  $r_+ = 5.00$  and  $\nu = 0$  there are two purely dissipative modes with the smallest imaginary parts. For non-zero  $\nu$  these modes approach each other until finally, at  $\nu = 0.0663$ , they take on the same value and they acquire non-vanishing real parts, transforming into propagating QNMs. We obtain agreement with the asymptotic analytic expression (3.53) for  $\nu = 0$  ( $\Im\omega = -7.50, -15$  for  $r_+ = 5.00$ ).

For intermediate horizons, such as  $r_+ = 1.50$ , the picture is different: the purely dissipative modes have relatively small absolute values for  $\nu = 0.40$  and their absolute values increase as one approaches  $\nu = 0$ . We note that for  $\nu = 0$  there are no purely dissipative modes at all for this value of  $r_+$ , so it appears that the imaginary parts of the QNMs tend to  $-\infty$  as  $\nu \rightarrow 0$ . This is in agreement with the modes obtained by solving the exact analytic equation (3.52) which is valid for  $\nu = 0$ .

The QNMs for  $Z_1$  perturbations fall into two disjoint classes; they belong to either large horizons ( $r_+ > 3.15$ ) or small ones ( $r_+ < 3.15$ ). They have different properties for  $\nu = 0$ : large horizons have purely imaginary modes in this limit, while small ones do not. The behaviours of the two classes are qualitatively different.

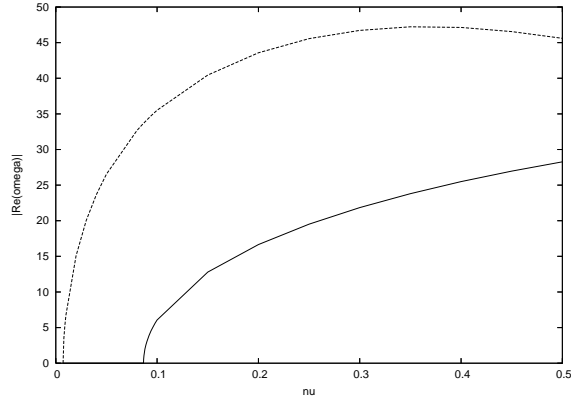


Figure 4: The (absolute) real part of the axial  $Z_1$  QNMs with  $r_+ = 20.00$  versus fractional charge  $\nu$ . The corresponding  $\lambda$  ranges from 0 to 0.05. The solid line corresponds to the real part of the lowest  $Z_1$  mode; the dashed line is the real part of the second lowest  $Z_1$  mode.

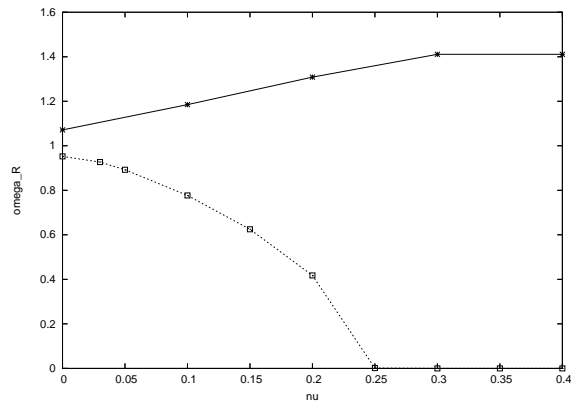


Figure 5: The (absolute) real parts of the axial  $Z_1$  (lower curve) and  $Z_2$  lowest modes at  $r_+ = 0.95$  versus fractional charge  $\nu$ .

If we go now to a horizon close to and below the critical point,  $r_+ = 0.995$  (Fig. 10), we have in some sense the reverse behaviour: a finite number of propagating modes corresponds to the smallest absolute values of the imaginary part, a positive slope is observed and finally purely dissipative modes appear with large imaginary parts. For small  $\nu$  we observe the phenomenon just described, the propagating modes appearing last; for somewhat larger  $\nu$  purely dissipative and propagating QNMs are mixed. An important point is that the  $\nu \rightarrow 0$  limit of the imaginary parts is finite for  $r_+ = 0.995$ , in contrast to what happens for the intermediate value  $r_+ = 1.50$  (Fig. 9).

### 5.1.1 Temperature Dependence

An issue that should be examined is the  $r_+$ –dependence of the imaginary parts. It turns out that it is advantageous to use the temperature rather than  $r_+$  as a variable: in Fig. 11 we depict the (absolute value of the) imaginary part of the purely dissipative modes corresponding to zero charge for large horizons versus the temperature. We observe that the

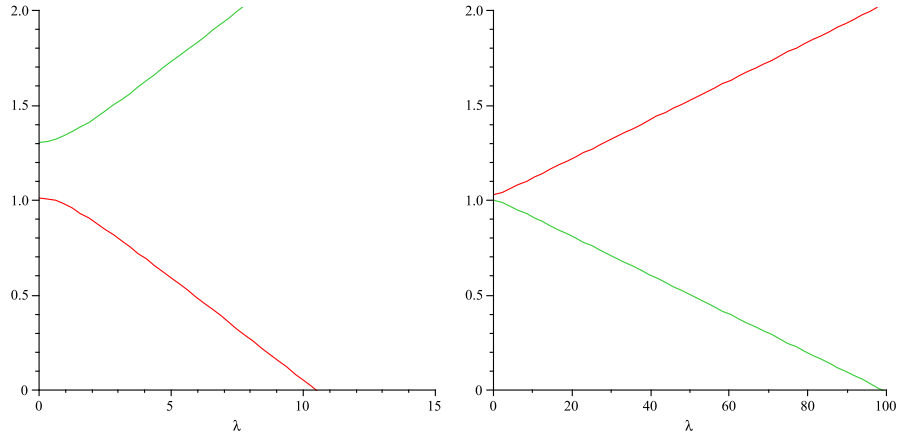


Figure 6: The (absolute) real parts of the axial  $Z_1$  (lower curve) and  $Z_2$  lowest modes at  $r_+ = 0.95$  and  $r_+ = 0.995$  versus  $\lambda$  using the analytical expressions (3.36) and (3.43).

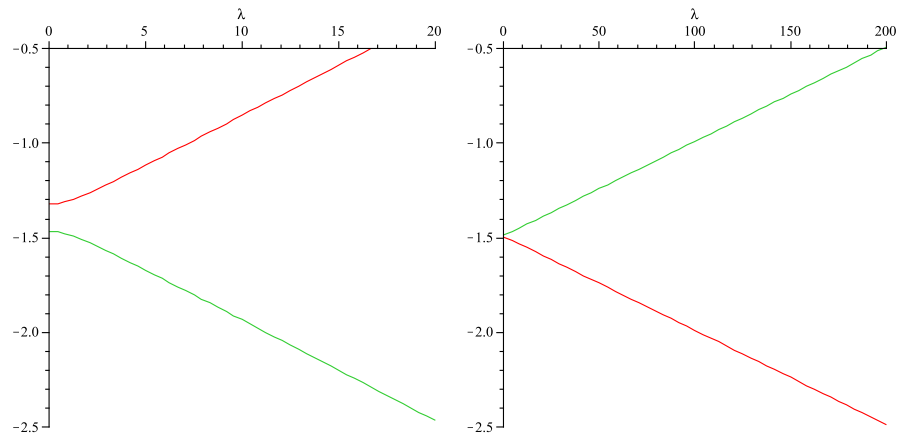


Figure 7: The imaginary parts of the axial  $Z_1$  (upper curve) and  $Z_2$  lowest modes at  $r_+ = 0.95$  and  $r_+ = 0.995$  versus  $\lambda$  using the analytical expressions (3.36) and (3.43).

imaginary parts scale linearly with the temperature to high accuracy. The data points have been calculated numerically as well as by solving the exact analytic equation (3.52), the two results being in excellent agreement with each other. The linear fits agree with the analytic asymptotic expression (3.53).

We also examined the intermediate horizons, in particular  $r_+ = 0.90$  up to  $r_+ = 2.00$  with  $\lambda = 0.50$ . The relevant temperature  $T - T_0$  ranges from  $-0.04$  to  $0.24$ . The two lowest modes are depicted in Fig. 12. Good quality fits ( $\chi_{d.o.f.}^2 < 1$ ) of the form  $a + \frac{b}{T - T_0}$  are possible for both branches:  $T > T_0$  and  $T < T_0$ . The curves for the lowest modes are also included in the figure. We observe that there is an (infinite!) change in the slope of this graph at  $T = T_0$ , which presumably signals a phase transition.

In Fig. 13, we show a similar plot in the case of no charge but this time using the exact analytic eq. (3.53). We obtain a similar singular behaviour ( $\Im\omega \sim (T - T_0)^{-1}$ ) reinforcing the conclusion that a phase transition occurs at  $T = T_0$ .

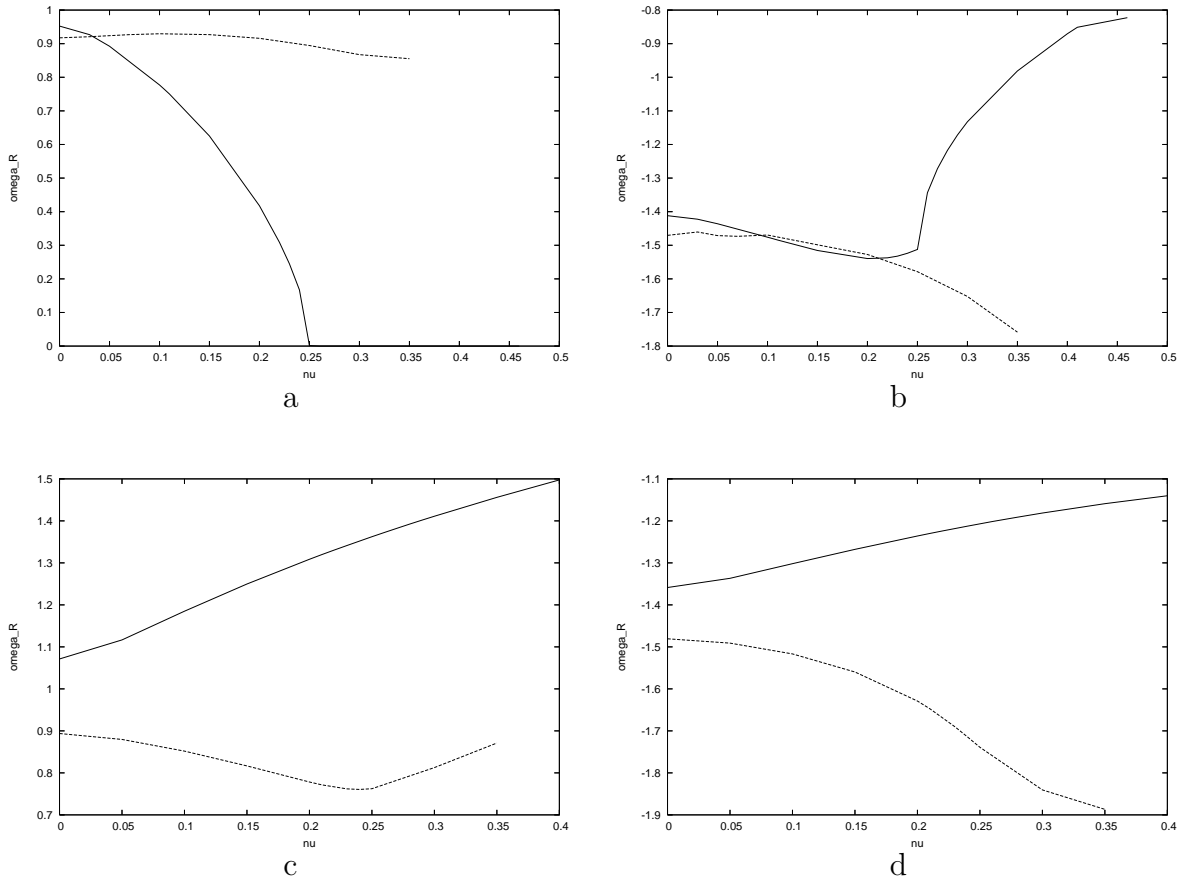


Figure 8: Panel (a): The real parts of the lowest QNMs of the axial (lower curve) and polar (upper curve) perturbations for  $Z_1$  versus  $\nu$  at  $r_+ = 0.95$ . Panel (b): The imaginary parts of the lowest QNMs of the axial (upper curve) and polar (lower curve) perturbations for  $Z_1$  versus  $\nu$  at  $r_+ = 0.95$ . The real, panel (c) and imaginary, panel (d), parts of the lowest QNMs of the axial (upper curve) and polar (lower curve) perturbations for  $Z_2$  versus  $\nu$  at  $r_+ = 0.95$ .

### 5.1.2 $\xi$ –Dependence

For large horizons (typical value  $r_+ = 5.00$ ) we consider the  $\nu = 0$  case. The  $\xi$ –dependence is shown in Fig. 14. As  $\xi$  grows, the purely dissipative modes converge towards each other and finally disappear (that is, they turn into propagating modes with finite real part), a behaviour strongly reminiscent of the  $\nu$ –dependence, depicted in Fig. 9. We have chosen to depict in Fig. 15 the  $\xi$ –dependence of the lowest QNM for a typical intermediate horizon. Numerical results are in excellent agreement with the results obtained by solving the exact analytic equation (3.52). In particular, for  $\xi = 0$ , we obtain the two values  $\Im\omega = -15, -7.50$  from eq. (3.53) whereas the two modes coalesce at the value  $\Im\omega = -10.25$  at  $\Lambda = 2.875$  corresponding to  $\xi = 1.62$  (eq. (3.54)), all in agreement with numerical results.

For  $r_+ = 0.995$ ,  $\nu = 0$  we know from the analytical calculations that the imaginary part

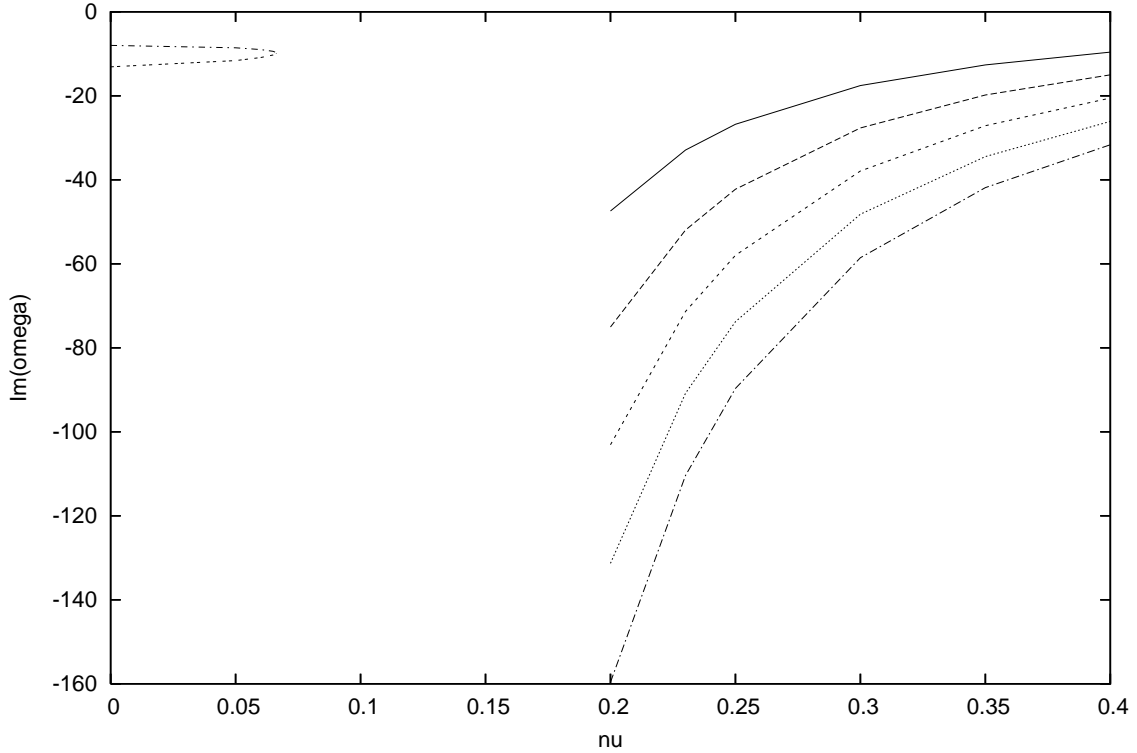


Figure 9: The imaginary part of the axial  $Z_1$  purely dissipative QNMs with  $r_+ = 5.00$  (upper left corner), the corresponding  $\lambda$  being smaller than 0.042 and  $r_+ = 1.50$  (right part of the figure) versus fractional charge  $\nu$ , the corresponding  $\lambda$  ranging between 0.65 and 0.90.

of the QNMs changes little, so we focus on the  $\xi$ -dependence of their real parts. We confirm numerically that the change in the imaginary parts is small and calculate numerically the real parts. The results for the lowest QNMs are shown in Fig. 16. Both numerical and analytical results (eq. (3.43)) are shown for comparison.

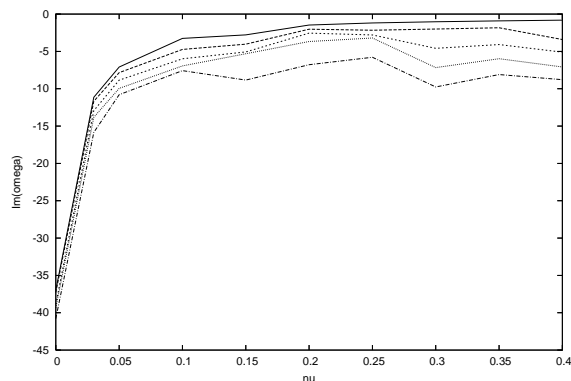


Figure 10:  $Im(\omega)$  versus  $\nu$  for the five lowest  $Z_1$  purely dissipative modes at  $r_+ = 0.995$ .

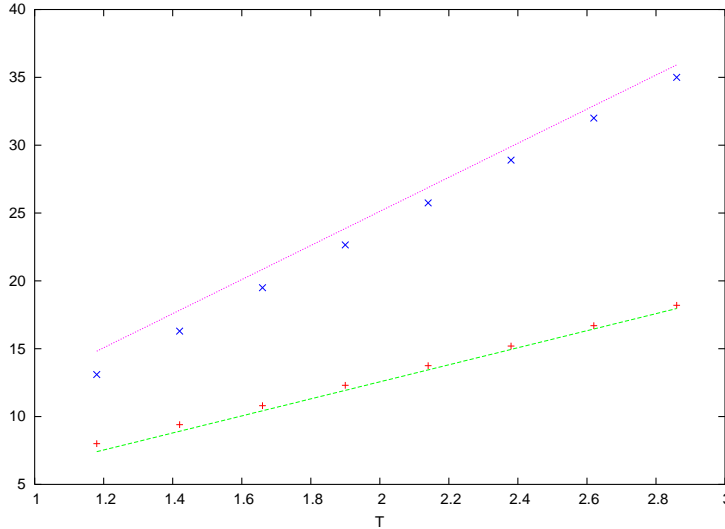


Figure 11: The (absolute value of the) imaginary part of the two  $Z_1$  purely dissipative QNMs with  $\nu = 0$ ,  $\xi = 1$  versus temperature. Horizons vary from  $r_+ = 5.00$  to  $r_+ = 12.00$ . Also shown are the asymptotic expressions (3.53).

We observe that the real parts decrease with decreasing  $\xi$  until they vanish at some critical value. For  $\xi$  smaller than this critical value, the QNMs will be pure imaginary. The critical values of  $\xi$  given by the analytic expressions (3.47) are in good agreement with numerical results. This is seen in Fig. 17 which shows the singular behaviour of the three lowest critical values of  $\xi$  just below the critical point  $T = T_0$ . The data points have been calculated both numerically and by using the analytic equation (3.52).

For a given  $\xi$ , the corresponding modes will be purely dissipative for large enough  $\Im\omega$ , since the relevant curve will have crossed the axis at a value greater than the given  $\xi$ ; however there will exist in general curves (that is, appropriate values of  $\Im\omega$ ), for which the corresponding  $\Re\omega$  will be different from zero and the QNM will be a propagating one. Therefore, QNMs with a sufficiently large absolute value of the imaginary part will be purely dissipative, while the lowest QNMs will be propagating. This calculation confirms once again that the lowest QNMs will be propagating, followed by purely dissipative ones. This fully agrees with the numerical results for small horizons and zero charge. The situation is exactly the opposite for large horizons: in that case the curves of approximately constant imaginary part never cross the horizontal axis. For non-zero values of the charge the picture is similar.

## 5.2 Axial $Z_2$ Perturbations

The results are described starting in Fig. 18 which provides a picture similar in some respects to the corresponding result for  $Z_1$  excitations shown in Fig. 9. Two differences should be noted, however: (a) There is no qualitative distinction between intermediate and large horizons here. In particular, there is no need to also depict the behaviour of  $r_+ = 5.00$ , as we did in Fig. 9, and (b) the absolute value of the lowest QNM is much smaller than



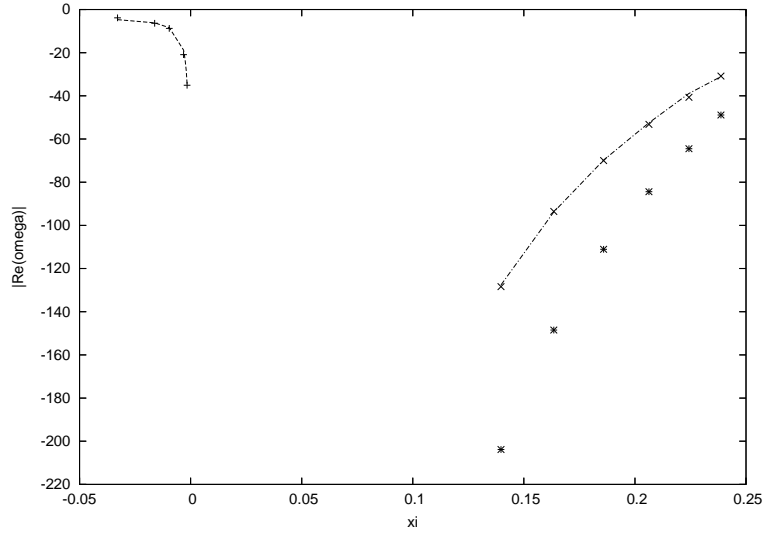


Figure 12: The imaginary parts of the two lowest axial  $Z_1$  purely dissipative QNMs with  $\lambda = 0.50$  versus temperature. For  $T < T_0$  the lowest modes are represented by points, while the second lowest ones with lines. For  $T > T_0$  the lowest modes are represented by points and lines, while the second lowest ones with points. Horizons vary from  $r_+ = 0.90$  to  $r_+ = 2.00$ .

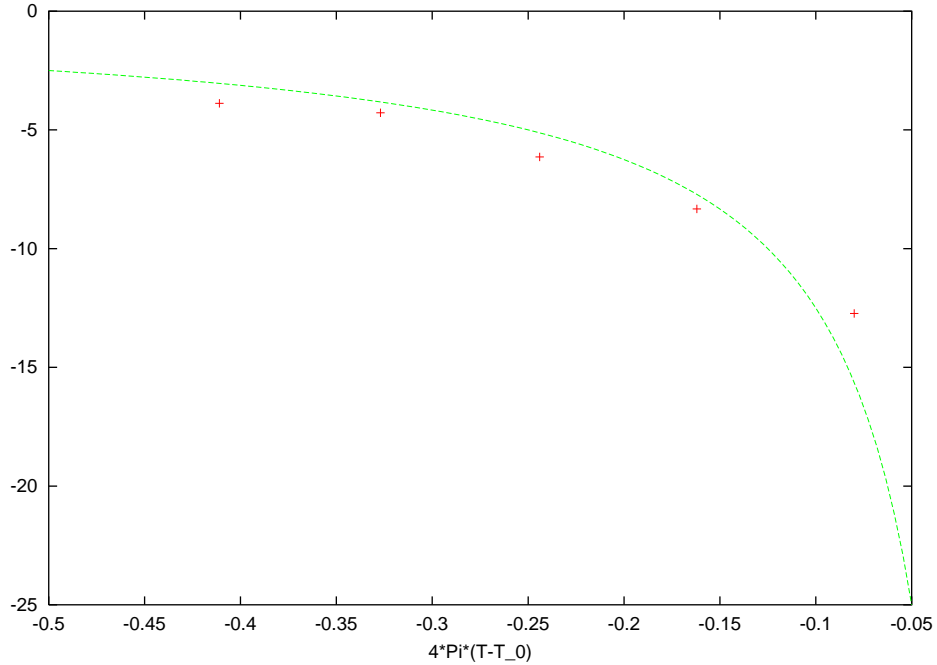


Figure 13: The imaginary part of the lowest frequency  $\omega_0$  of the axial  $Z_1$  purely dissipative mode versus temperature for  $\lambda = 0$ ,  $\xi = 1$  from the exact analytic eq. (3.53). Also shown is a fit  $\Im\omega_0 = \frac{1.25}{4\pi(T-T_0)}$ .

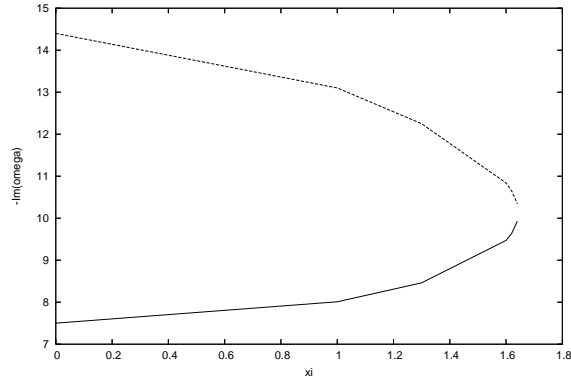


Figure 14: The imaginary part of the two  $Z_1$  purely dissipative QNMs for  $r_+ = 5.00$ ,  $\nu = 0$  versus  $\xi$ .

the remaining ones; it almost coincides with the horizontal axis.

For small horizons we have chosen to depict the results for  $r_+ = 0.995$  in Fig. 19. The picture is qualitatively the same as the corresponding result for  $Z_1$  excitations, shown in Fig. 10. In particular, nothing is special about the lowest mode in this case: this should be contrasted with the results above the critical point presented previously in Fig. 18.

### 5.2.1 Temperature Dependence

Next we examine the temperature (or horizon) dependence of axial  $Z_2$  modes. Fig. 20 contains the numerical results for the two lowest purely dissipative modes versus  $T - T_0$  for  $\lambda = 0.50$ . The lowest mode has been reported in [5, 7] to scale as  $\frac{1}{r_+}$  which agrees with our analytic asymptotic expression (3.31). Using the temperature, rather than the horizon, as

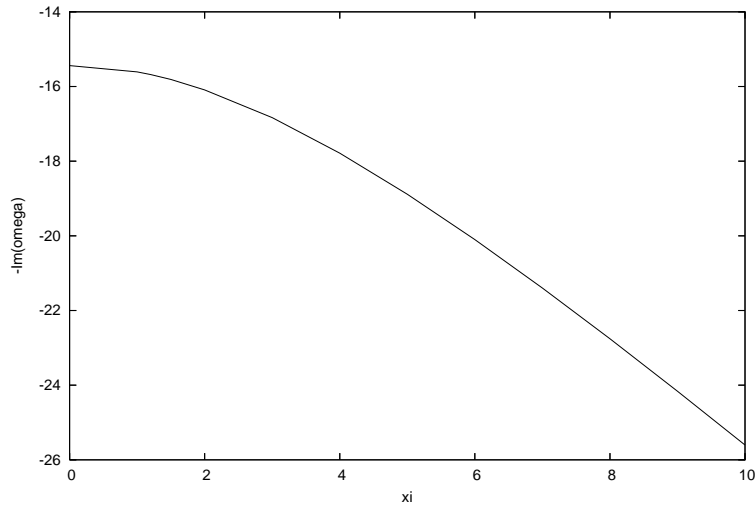


Figure 15: The imaginary part of the axial lowest  $Z_1$  purely dissipative QNMs with  $r_+ = 2.00$  and  $\nu = 0.40$  versus  $\xi$ .

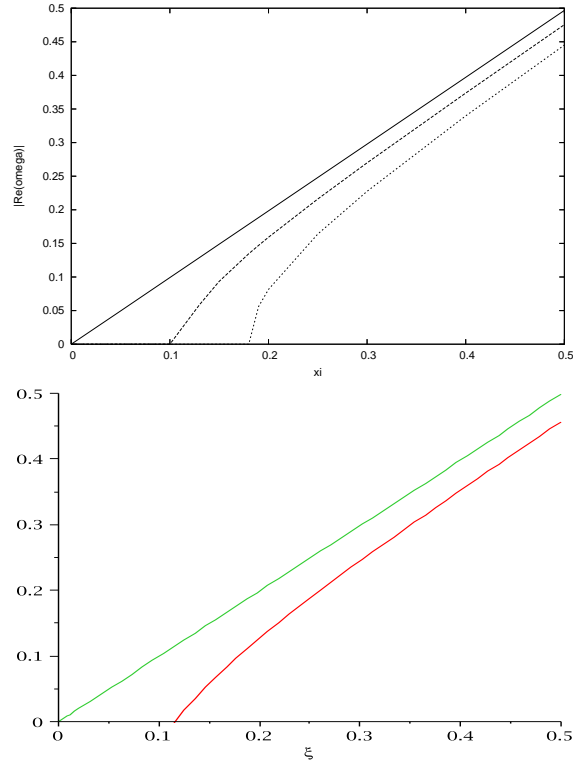


Figure 16: The real part of the four lowest axial  $Z_1$  QNMs with  $r_+ = 0.995$  versus the  $\xi$  parameter for  $\nu = 0.00$ . The imaginary part decreases from left to right. The second panel shows the analytical estimate for the lowest two modes (eq. (3.43)) for comparison.

an independent variable, we have found that this mode scales as  $a + \frac{b}{T-T_0}$  above the critical temperature; this fit is of very good quality and is shown in the figure. However, we have not been able to fit the  $T < T_0$  data to a function of this form except very close to the critical point  $T = T_0$ . There is an infinite change in slope at the critical temperature, as in the  $Z_1$  case. We also remark that for  $T < T_0$  the two lowest values are very close to each other, while for  $T > T_0$  we have a lowest mode with a very small absolute value, while the absolute value of the second lowest mode is much larger.

The above conclusions are confirmed by our analytic results. In Fig. 21, we show the lowest mode for  $\lambda = 0$  for various temperatures both above and below the critical point. The data points were found by solving the analytic equation (3.57). Once again, we observe a singular behaviour characterized by an infinite change in the slope at the critical point.

### 5.2.2 $\xi$ –Dependence

We now proceed with a discussion of the  $\xi$ –dependence for the two regimes: large and small horizons. Fig. 22 contains both numerical and analytic results (using the asymptotic expression (3.31)) for  $r_+ = 20.00$ . The value  $\xi = 0$  yields the uppermost curve. This behaviour is similar to the behaviour for intermediate horizons in the axial  $Z_1$  case (Fig. 15)

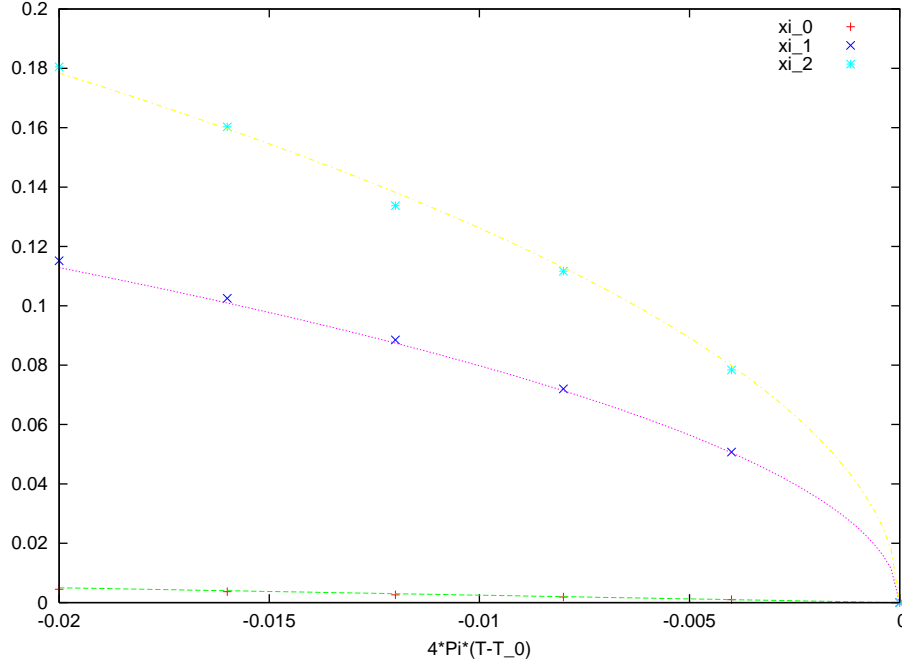


Figure 17: The first three critical values of  $\xi$  for axial  $Z_1$  modes versus temperature for  $\nu = 0$ . Also shown are fits,  $\xi_0 = \pi(T_0 - T)$ ,  $\xi_1 = \sqrt{8(T_0 - T)}$ ,  $\xi_2 = \sqrt{20(T_0 - T)}$ .

and is quite different from the behaviour for large horizons in that case (Fig. 14).

For horizons below the critical point, results are contained in Fig. 23 where we chose a value close to the critical point,  $r_+ = 0.995$ . The results are slightly different from the  $Z_1$  case (Fig. 16). In fact, the real part initially increases, it attains a maximal value and then it decreases and cuts the axis. This happens for very large values of the imaginary part, of the order of 30, the exact value depending on  $\xi$ . Coming back to Fig. 23, the lowest plotted curve corresponds to such a value. We have also plotted the analytic results

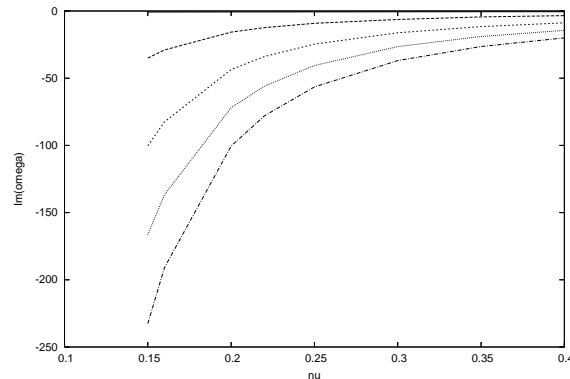


Figure 18:  $\Im\omega$  versus fractional charge  $\nu$  for the five lowest  $Z_2$  purely dissipative modes at  $r_+ = 1.50$ .

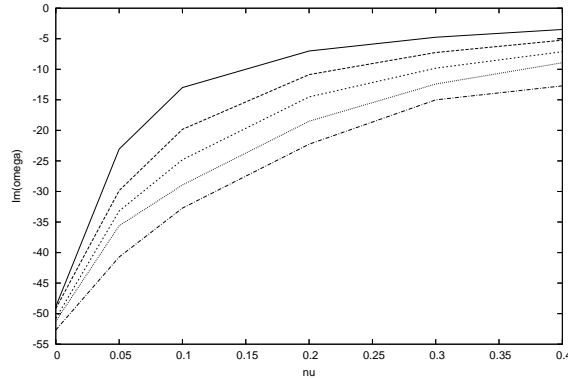


Figure 19: The imaginary part of the axial  $Z_2$  purely dissipative QNMs at  $r_+ = 0.995$  versus fractional charge  $\nu$ .

(3.36) and (3.43). The agreement with the numerical results is good when  $\xi$  is not small. As  $\xi \rightarrow 0$ , the corrections (3.43) exceed the zeroth order result (3.36) and the first-order approximation fails.

For comparison, we also show results slightly above the critical point in Fig. 24 where we chose  $r_+ = 1.005$  and  $\nu = 0$ . Here the behaviour is very similar to the behaviour of  $Z_1$  modes slightly *below* the critical points (*cf.* with Fig. 16). Similar remarks can be made in this case. For each mode, there exists a critical value of  $\xi$  below which the mode does not propagate and becomes purely dissipative ( $\Re\omega = 0$ ). These critical values of  $\xi$  depend on the temperature. Their behaviour near the critical temperature is given by the analytic expressions (3.45), (3.46) and plotted in Fig. 25 (*cf.* with Fig. 17 for  $Z_1$  modes). Data points were found numerically as well as by solving the analytical equation (3.57).

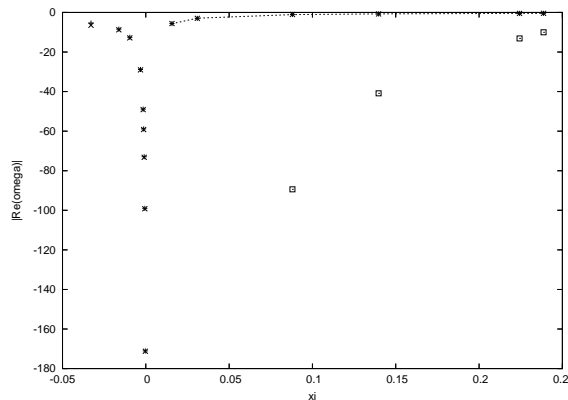


Figure 20:  $\Im\omega$  versus  $T - T_0$  for the lowest and second lowest axial  $Z_2$  modes at  $\lambda = 0.50$ . For  $T < T_0$  the lowest modes are represented by a line just connecting the points, while the second lowest ones with points. For  $T > T_0$  the lowest modes are represented by a fit and the points, while the second lowest ones with points. Horizon values vary from  $r_+ = 0.90$  to 2.00.

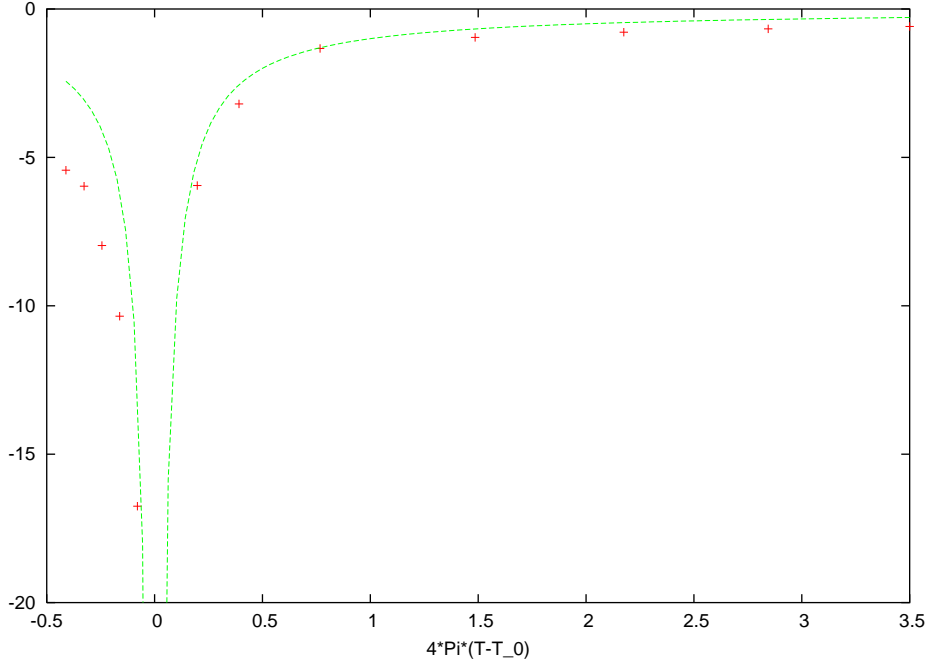


Figure 21: The imaginary part of the lowest frequency  $\omega_0$  of the axial  $Z_2$  purely dissipative mode versus temperature for  $\xi = 1$ . Also shown is a fit  $\Im\omega_0 = -\frac{1}{4\pi|T-T_0|}$ .

## 6 Conclusions

We have studied the perturbative behaviour of the charged topological black holes. We have calculated both analytically and numerically the QNMs of electromagnetic and gravitational perturbations of these black holes.

For large black holes we found analytically that the axial  $Z_2$  QNMs are purely dissipative, depend on the charge and scale as the inverse of the black hole horizon. The  $Z_1$  axial modes are proportional to the black hole horizon but analytical expressions cannot be obtained in general for non-zero charge. For zero charge the potentials for both axial and polar modes reduce to electromagnetic potential and the wave function can be written in terms of the Heun function, leading to a semi-analytic expressions of the QNMs.

For small black holes, at the critical point with zero charge and mass the wave equation simplifies and the QNMs can be explicitly calculated. For small changes around the critical point, the real part of the  $Z_2$  modes increases above the critical point giving a positive slope, whereas below the critical point it gives a negative slope. Above the critical point, for these modes there is a critical value of  $\xi$  below which there are only purely dissipative modes. Below the critical point, there are no purely dissipative modes for any value of  $\xi$ . The  $Z_1$  modes exhibit the opposite behaviour. Similar behaviour is exhibited by the polar modes.

These results are also supported by numerical investigations of the QNMs. The numerical results show clearly a change of slope of QNMs around a critical temperature for all

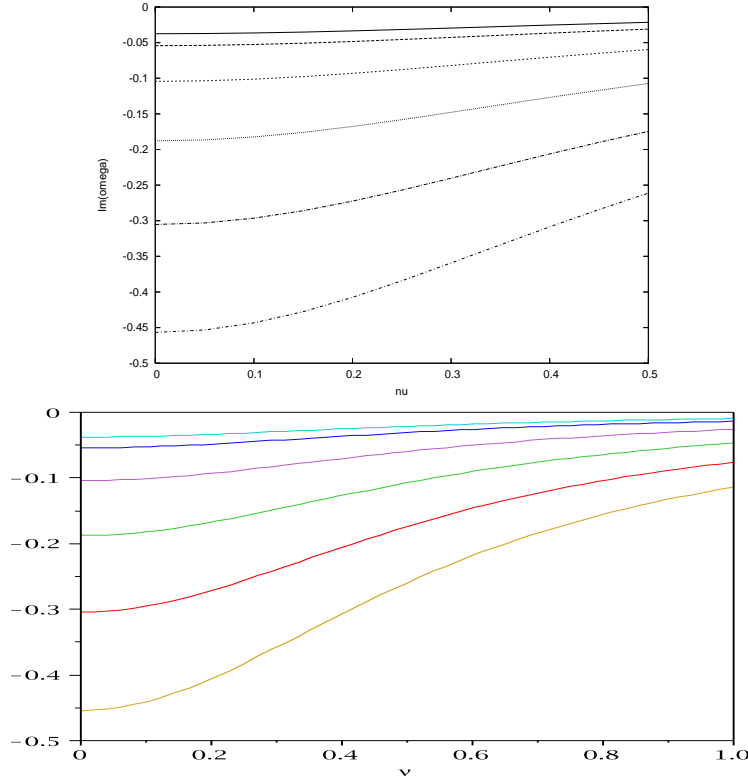


Figure 22:  $\Im\omega$  versus fractional charge  $\nu$  for the lowest purely dissipative mode of axial  $Z_2$  perturbations at  $r_+ = 20.00$ . The corresponding  $\lambda$  is smaller than 0.15. The curves correspond to (top to bottom)  $\xi = 0, 1, 2, 3, 4, 5$ . The second panel shows the analytical expression for comparison.

kinds of perturbations. We found that the purely dissipative modes scale linearly with temperature for large black holes, while for small horizons they scale according to  $a + b/(T - T_0)$ . Then, for a fixed charge to mass ratio we observed an infinite change of slope at  $T = T_0$  signaling a second order phase transition.

The numerical results show also an interesting dependence of the modes on the charge of the black hole. For small horizons and small charge the number of propagating ( $\Re\omega \neq 0$ ) QNMs is finite, while as the charge increases, positive slope frequencies coexist with frequencies of negative slope and the number of propagating QNMs is again infinite. As the charge increases, a drastic change in the temperature dependence occurs.

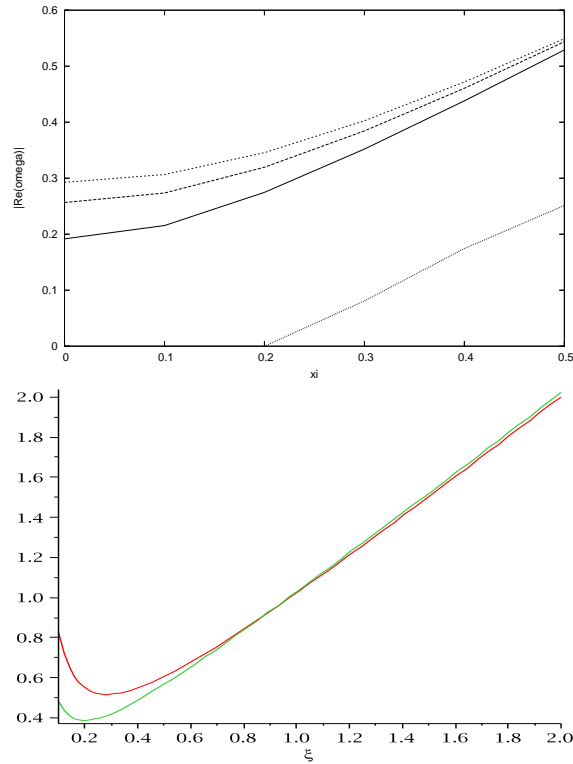


Figure 23: The (absolute values of the) real parts of  $Z_2$  modes versus  $\xi$  at  $r_+ = 0.995$ . The curves correspond to the values (top to bottom)  $\Im\omega = -5.45, -3.47, -1.49, -29.21$ . The second panel shows the analytic approximation for the lowest two modes.

## Acknowledgments

Work supported by the NTUA research program PEVE07. E. P. was partially supported by the European Union through the Marie Curie Research and Training Network UniverseNet (MRTN-CT-2006-035863). G. S. was supported in part by the US Department of Energy under grant DE-FG05-91ER40627.

## References

- [1] K. D. Kokkotas and B. G. Schmidt, Living Rev. Rel. **2**, 2 (1999) [arXiv:gr-qc/9909058].
- [2] H.-P. Nollert, H. P. Nollert, Class. Quant. Grav. **16** (1999) R159.
- [3] J. S. F. Chan and R. B. Mann, Phys. Rev. D **55**, 7546 (1997) [arXiv:gr-qc/9612026]; Phys. Rev. D **59**, 064025 (1999).
- [4] G. T. Horowitz and V. E. Hubeny, Phys. Rev. D **62**, 024027 (2000) [arXiv:hep-th/9909056].
- [5] V. Cardoso and J. P. S. Lemos, Phys. Rev. D **64**, 084017 (2001) [arXiv:gr-qc/0105103].



- [6] B. Wang, C. Y. Lin and E. Abdalla, Phys. Lett. B **481**, 79 (2000) [arXiv:hep-th/0003295].
- [7] E. Berti and K. D. Kokkotas, Phys. Rev. D **67**, 064020 (2003) [arXiv:gr-qc/0301052].
- [8] F. Mellor and I. Moss, Phys. Rev. D **41**, 403 (1990).
- [9] R. A. Konoplya, Phys. Rev. D **66**, 044009 (2002) [arXiv:hep-th/0205142]; V. Cardoso, R. Konoplya and J. P. S. Lemos, Phys. Rev. D **68**, 044024 (2003) [arXiv:gr-qc/0305037].
- [10] J. M. Maldacena, Adv. Theor. Math. Phys. **2**, 231 (1998) [Int. J. Theor. Phys. **38**, 1113 (1999)] [arXiv:hep-th/9711200]; E. Witten, Adv. Theor. Math. Phys. **2**, 253 (1998) [arXiv:hep-th/9802150]; S. S. Gubser, I. R. Klebanov and A. M. Polyakov, Phys. Lett. B **428**, 105 (1998) [arXiv:hep-th/9802109].
- [11] S. Hawking and D. Page, Commun. Math. Phys. **87** (1983) 577.
- [12] E. Witten, Adv. Theor. Math. Phys. **2**, 505 (1998) [arXiv:hep-th/9803131].

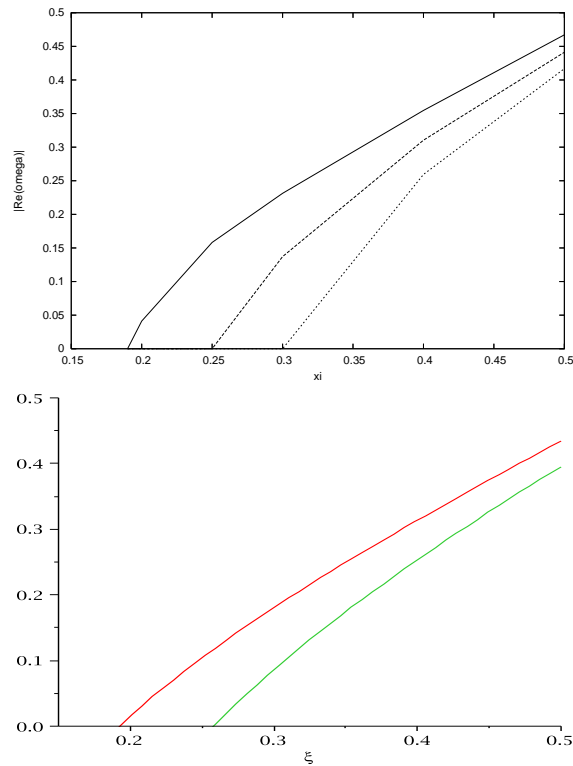


Figure 24: The (absolute values of the) real parts of the  $Z_2$  axial modes versus  $\xi$  at  $r_+ = 1.005$ ,  $\nu = 0$ . The imaginary part decreases from left to right. The second panel shows the analytic estimate (eq. (3.43)) for the two lowest modes.

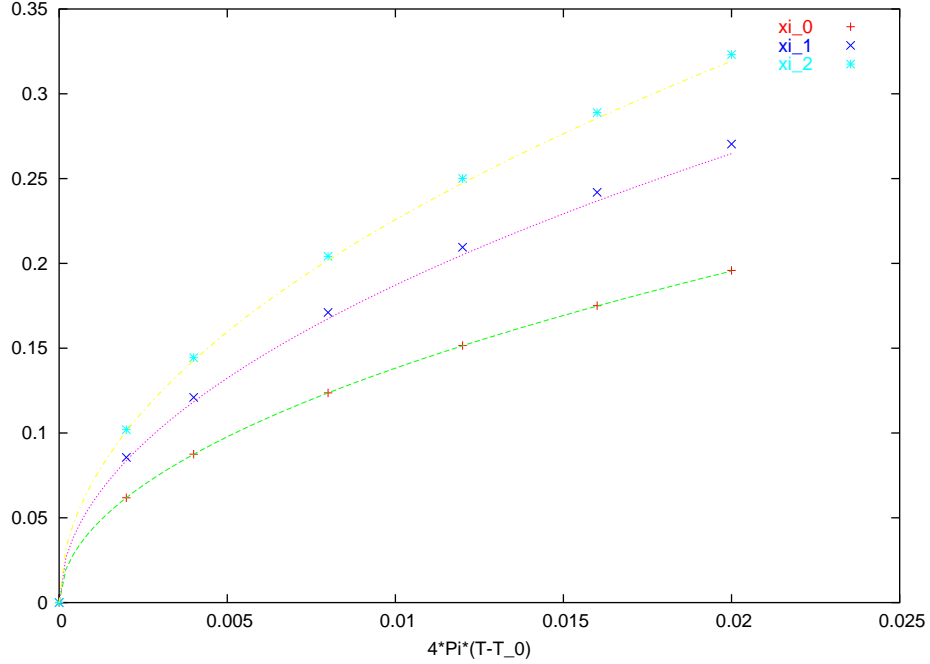


Figure 25: The first three critical values of  $\xi$  for axial  $Z_2$  modes versus temperature for  $\nu = 0$ . Also shown are fits,  $\xi_0 = \sqrt{24(T - T_0)}$ ,  $\xi_1 = \sqrt{46(T - T_0)}$ ,  $\xi_2 = \sqrt{64(T - T_0)}$ .

- [13] C. Martinez, R. Troncoso and J. Zanelli, Phys. Rev. D **70**, 084035 (2004) [arXiv:hep-th/0406111].
- [14] G. Koutsoumbas, S. Musiri, E. Papantonopoulos and G. Siopsis, JHEP **0610**, 006 (2006) [arXiv:hep-th/0606096].
- [15] J. Shen, B. Wang, C. Y. Lin, R. G. Cai and R. K. Su, JHEP **0707**, 037 (2007) [arXiv:hep-th/0703102]; X. Rao, B. Wang and G. Yang, Phys. Lett. B **649**, 472 (2007) [arXiv:0712.0645 [gr-qc]].
- [16] R. B. Mann, Class. Quant. Grav. **14**, L109 (1997) [arXiv:gr-qc/9607071]; R. B. Mann, Nucl. Phys. B **516**, 357 (1998) [arXiv:hep-th/9705223].
- [17] L. Vanzo, Phys. Rev. D **56**, 6475 (1997) [arXiv:gr-qc/9705004].
- [18] J. P. S. Lemos and V. T. Zanchin, Phys. Rev. D **54**, 3840 (1996) [arXiv:hep-th/9511188]; J. P. S. Lemos, Phys. Lett. B **353**, 46 (1995) [arXiv:gr-qc/9404041].
- [19] D. R. Brill, J. Louko and P. Peldan, Phys. Rev. D **56**, 3600 (1997) [arXiv:gr-qc/9705012].
- [20] D. Birmingham, Class. Quant. Grav. **16**, 1197 (1999) [arXiv:hep-th/9808032].

- [21] G. Gibbons and S. A. Hartnoll, Phys. Rev. D **66**, 064024 (2002) [arXiv:hep-th/0206202].
- [22] D. Birmingham and S. Mokhtari, Phys. Rev. D **76**, 124039 (2007) [arXiv:0709.2388 [hep-th]].
- [23] R. Aros, C. Martinez, R. Troncoso and J. Zanelli, Phys. Rev. D **67**, 044014 (2003) [arXiv:hep-th/0211024].
- [24] Y. S. Myung, Phys. Lett. B **645**, 369 (2007) [arXiv:hep-th/0603200]; arXiv:0801.2434 [hep-th].
- [25] D. Birmingham and S. Mokhtari, Phys. Rev. D **74**, 084026 (2006) [arXiv:hep-th/0609028]; A. Sheykhi, arXiv:0709.3619 [hep-th]; M. Nadalini, L. Vanzo and S. Zerbini, arXiv:0710.2474 [hep-th].
- [26] R. Emparan, JHEP **9906**, 036 (1999) [arXiv:hep-th/9906040].
- [27] R. Emparan, Phys. Lett. B **432**, 74 (1998) [arXiv:hep-th/9804031].
- [28] C. Martinez, J. P. Staforelli and R. Troncoso, Phys. Rev. D **74**, 044028 (2006) [arXiv:hep-th/0512022].
- [29] H. Kodama and A. Ishibashi, Prog. Theor. Phys. **110**, 701 (2003) [arXiv:hep-th/0305147]; H. Kodama and A. Ishibashi, Prog. Theor. Phys. **111**, 29 (2004) [arXiv:hep-th/0308128].
- [30] G. Michalogiorgakis and S. S. Pufu, JHEP **0702**, 023 (2007) [arXiv:hep-th/0612065].
- [31] G. Siopsis, JHEP **0705**, 042 (2007) [arXiv:hep-th/0702079].